Pyrolysis of Oxalate, Acetate, and Perchlorate Mixtures and the Implications for Organic Salts on Mars

J. M. T. Lewis, J. L. Eigenbrode, G. M. Wong, A. C. Mcadam, P. D. Archer, B. Sutter, Maeva Millan, R. H. Williams, Melissa Guzman, A. Das, et al.

JGR Planets

RESEARCH ARTICLE

10.1029/2020JE006803

Pyrolysis of Oxalate, Acetate, and Perchlorate Mixtures and the Implications for Organic Salts on Mars

J. M. T. Lewis[1,2,3], J. L. Eigenbrode[2], G. M. Wong[4], A. C. McAdam[2], P. D. Archer[5], B. Sutter[5], M. Millan[2,6], R. H. Williams[2,3,7], M. Guzman[8], A. Das[9], E. B. Rampe[10], C. N. Achilles[2,11], H. B. Franz[2], S. Andrejkovičová[12], C. A. Knudson[2,3,7], and P. R. Mahaffy[2]

[1]Department of Physics and Astronomy, Howard University, Washington, DC, USA, [2]NASA Goddard Space Flight Center, Greenbelt, MD, USA, [3]Center for Research and Exploration in Space Science and Technology, NASA GSFC, Greenbelt, MD, USA, [4]Department of Geosciences, The Pennsylvania State University, University Park, PA, USA, [5]Jacobs, NASA Johnson Space Center, Houston, TX, USA, [6]Department of Biology, Georgetown University, Washington, DC, USA, [7]Center for Research and Exploration in Space Science and Technology, University of Maryland, College Park, MD, USA, [8]LATMOS/IPSL, UVSQ Université Paris-Saclay, Sorbonne Université, CNRS, Guyancourt, France, [9]International Space University, Strasbourg, France, [10]NASA Johnson Space Center, Houston, TX, USA, [11]Universities Space Research Association, Columbia, MD, USA, [12]Geosciences Department, GEOBIOTEC Unit, Aveiro University, Aveiro, Portugal

Abstract Organic salts, such as Fe, Ca, and Mg oxalates and acetates, may be widespread radiolysis and oxidation products of organic matter in Martian surface sediments. Such organic salts are challenging to identify by evolved gas analysis but the ubiquitous CO_2 and CO in pyrolysis data from the Sample Analysis at Mars (SAM) instrument suite on the Curiosity rover indirectly points to their presence. Here, we examined laboratory results from SAM-like analyses of organic salts as pure phases, as trace phases mixed with silica, and in mixtures with Ca and Mg perchlorates. Pure oxalates evolved CO_2 and CO, while pure acetates evolved CO_2 and a diverse range of organic products dominated by acetone and acetic acid. Dispersal within silica caused minor peak shifting, decreased the amounts of CO_2 evolved by the acetate standards, and altered the relative abundances of the organic products of acetate pyrolysis. The perchlorate salts scrubbed Fe oxalate CO releases and shifted the CO_2 peaks to lower temperatures, whereas with Ca and Mg oxalate, a weaker CO release was observed but the initial CO_2 evolutions were largely unchanged. The perchlorates induced a stronger CO_2 release from acetates at the expense of other products. Oxalates evolved ~47% more CO_2 and acetates yielded ~69% more CO_2 when the perchlorates were abundant. The most compelling fits between our organic salt data and SAM CO_2 and CO data included Martian samples acquired from modern eolian deposits and sedimentary rocks with evidence for low-temperature alteration.

Plain Language Summary In our efforts to characterize indigenous Martian organic matter, we must contend with a near-surface record that has been substantially altered by radiation and oxidation. Under such conditions, much of the surficial organic record on Mars may have decomposed into organic salts, which are challenging for flight instruments to conclusively identify. If organic salts are widespread on the Martian surface, their composition and distribution could offer insight into the less-altered organic record at depth and they may play an important role in near-surface carbon cycling and habitability. The organic detection techniques employed by the Mars Science Laboratory Curiosity rover include thermal extraction in combination with mass spectrometry. In this work, we used laboratory thermal extraction techniques analogous to those of the rover to examine organic salts as pure standards, as minor phases in a silica matrix, and in mixtures with O_2-evolving perchlorate salts. When we compared our results with flight data, we found that many of the CO_2 profiles produced by our organic salt samples were similar to the CO_2 evolutions observed by the rover. The best fits with our laboratory data included Martian materials acquired from modern eolian deposits and sedimentary rocks that had evidence for low-temperature alteration.

Key Points:

- Flight-like thermal analyses of organic salts suggest such phases may have been present in many of the samples analyzed by Mars missions
- Perchlorates greatly impacted the thermal decomposition of organic salts and enhanced CO_2 production at the expense of other products
- The most compelling hints of organic salts occurred in pyrolysis data from altered Martian sedimentary rocks and modern eolian deposits

Supporting Information:

Supporting Information may be found in the online version of this article.

Correspondence to:

J. M. T. Lewis,
james.m.lewis@nasa.gov

Citation:

Lewis, J. M. T., Eigenbrode, J. L., Wong, G. M., McAdam, A. C., Archer, P. D., Sutter, B., et al. (2021). Pyrolysis of oxalate, acetate, and perchlorate mixtures and the implications for organic salts on Mars. *Journal of Geophysical Research: Planets*, *126*, e2020JE006803. https://doi.org/10.1029/2020JE006803

Received 21 DEC 2020
Accepted 26 FEB 2021

Author Contributions:

Conceptualization: J. M. T. Lewis, J. L. Eigenbrode, G. M. Wong
Data curation: J. M. T. Lewis, P. D. Archer, M. Millan
Formal analysis: J. M. T. Lewis, G. M. Wong, S. Andrejkovičová
Funding acquisition: J. L. Eigenbrode, P. R. Mahaffy

Investigation: J. M. T. Lewis, G. M. Wong, A. C. McAdam, P. D. Archer, B. Sutter, M. Millan, R. H. Williams, M. Guzman, A. Das, E. B. Rampe, C. N. Achilles, H. B. Franz, S. Andrejkovičová, C. A. Knudson
Methodology: J. M. T. Lewis, G. M. Wong, A. C. McAdam, H. B. Franz, S. Andrejkovičová
Project Administration: J. L. Eigenbrode
Resources: J. L. Eigenbrode
Software: G. M. Wong
Supervision: J. L. Eigenbrode, A. C. McAdam
Validation: G. M. Wong
Writing – original draft: J. M. T. Lewis, G. M. Wong, P. D. Archer, M. Millan, E. B. Rampe, C. N. Achilles
Writing – review & editing: J. M. T. Lewis, J. L. Eigenbrode, G. M. Wong, A. C. McAdam, P. D. Archer, B. Sutter, M. Millan, E. B. Rampe, C. N. Achilles, C. A. Knudson

1. Introduction

Organic matter preserved in the Martian rock record represents an invaluable resource for exploring the planet's carbon cycle, habitability, and potential biology through time. However, near-surface Martian organic matter is susceptible to transformation by ionizing radiation and oxidation (Benner et al., 2000; Biemann & Lavoie, 1979; Chun et al., 1978; Dartnell et al., 2012; Hassler et al., 2014; Lasne et al., 2016; Oró & Holzer, 1979; A. A. Pavlov et al., 2012; A. K. Pavlov et al., 2002; Poch et al., 2014). Flight instruments seeking to detect and characterize this near-surface organic record have utilized thermal extraction (pyrolysis) in combination with mass spectrometry (Biemann et al., 1976; Hoffman et al., 2008; Mahaffy et al., 2012). The Sample Analysis at Mars (SAM) instrument suite on board the Curiosity rover of the Mars Science Laboratory (MSL) mission at Gale crater has detected chlorinated hydrocarbons (Freissinet et al., 2015; Szopa et al., 2020) and other chemically diverse molecular components in the pyrolysis products of multiple samples, including products released at high temperatures (>500 °C) indicative of geologically refractory organic matter (Eigenbrode et al., 2018). Although the sources of these organic pyrolysis products have yet to be determined, these observations suggest preservation of organic matter over billions of years in Martian sediments (Eigenbrode et al., 2018).

Laboratory and field studies on Earth show that many organic compounds will decompose into metastable organic salts, such as oxalates and acetates, when exposed to radiation, oxidants, or volcanism (Applin et al., 2015; Benner et al., 2000; Echigo & Kimata, 2010; A. C. Fox et al., 2019; Hofmann & Bernasconi, 1998). Given that these processes may have significantly influenced the Martian organic record over billions of years, and that organic salts are known to persist in many terrestrial environments, it is of great importance that we better understand how organic salts behave under the analytical conditions of our flight experiments (Applin et al., 2015; Cheng et al., 2016; Dartnell, 2011; Dartnell et al., 2007, 2012; Hartmann et al., 1999; Hassler et al., 2014; Johnston & Vestal, 1993; Mahaffy et al., 2012; A. A. Pavlov et al., 2012; A. K. Pavlov et al., 2002). Analyses of Martian meteorites have revealed a suite of organic compounds with Martian D/H isotopic values in the shergottites NWA 1950 and Tissint, as well as the 1.3 Ga Nakhla meteorites, that include carbonyl and carboxyl group functionality and the Ca oxalate mineral whewellite was discovered in the Murchison meteorite (Fuchs et al., 1973; Steele et al., 2018). If organic salts are confirmed to be widespread on the Martian surface, their composition and distribution may offer insight into the less altered organic record at depth, as well as informing about near-surface carbon cycling and habitability. In this work, we examine how oxalates and acetates, existing as salts with Fe, Ca, and Mg cations, decompose during SAM-like pyrolysis, in order to assess if they are plausible phases in Gale crater sediments.

Investigating organic salts via thermal extraction is challenging as they produce simple pyrolysis products that can also be contributed by many other sources, such as the thermal decomposition of carbonates, the oxidation of more complex organic matter, or instrument backgrounds and contamination (Bamford & Tipper, 1980; Eigenbrode et al., 2018; Galwey & Brown, 1999; Sutter et al., 2017). Furthermore, additional CO_2, CO, O_2, H_2O, and catalysts in a pyrolysis oven can influence organic salt decomposition and many of the pyrolysis products can undergo side reactions (Bamford & Tipper, 1980; Bell et al., 1994; Judd et al., 1974; McAdie & Jervis, 1970).

Pyrolysis of metal oxalates is initiated by rupture of the C-C bond and typically results in formation of either the metal carbonate and CO (Reaction 1), the metal oxide, CO and CO_2 (Reaction 2), or the metal and CO_2 (Reaction 3) (Bamford & Tipper, 1980).

$$MC_2O_4(s) \rightarrow MCO_3(s) + CO(g) \quad \text{(R1)}$$

$$MC_2O_4(s) \rightarrow MO(s) + CO(g) + CO_2(g) \quad \text{(R2)}$$

$$MC_2O_4(s) \rightarrow M(s) + 2CO_2(g) \quad \text{(R3)}$$

An exception is Fe(III) oxalate, which according to Hermankova et al. (2010) yields a certain amount of Fe(II) oxalate during heating due to electron transfer to the Fe^{3+} cations (Reaction 4).

$$Fe_2(C_2O_4)_3(s) \rightarrow 2FeC_2O_4(s) + 2CO_2(g) \quad \text{(R4)}$$

Any remaining Fe(III) oxalate decomposes to Fe, Fe oxides, CO, and CO_2 between 220 °C and 320 °C. Between 300 °C and 390 °C Fe(II) oxalate decomposes to give Fe oxides, CO, and CO_2. Broadbent et al. (1967) performed X-ray analysis of the solid residue of Fe(III) oxalate decomposition after heating to 900 °C and found Fe, Fe_3O_4, and a trace of FeO. Hermankova et al. (2010) reported that Fe(III) oxalate decomposition does not take place in separate distinguishable steps under O_2, instead the formation of the Fe(II) oxalate intermediate and its decomposition to hematite occur almost simultaneously. They concluded that Fe^{3+} to Fe^{2+} reduction in Fe(III) oxalate decomposition is a general phenomenon caused by electron transfer that is atmosphere independent and that the amount of Fe(II) oxalate observed is instead dependent on its subsequent decomposition to hematite, which is controlled by the access of O_2 to the sample volume.

Kinetic studies of Mg oxalate decomposition indicate several overlapping reactions in the temperature range 420 °C–620 °C, which are the decomposition of the oxalate to $MgCO_3$ and CO, decomposition of $MgCO_3$ to MgO and CO_2, and oxidation of the CO to CO_2 if O_2 is present (Gadalla, 1984). In comparison, the decomposition of Ca oxalate to $CaCO_3$ and the dissociation of $CaCO_3$ to CaO are well separated steps (Bamford & Tipper, 1980; Gadalla, 1984; Lawson-Wood & Robertson, 2016). Some CO_2 may be observed during the decomposition of Ca oxalate to $CaCO_3$ due to the disproportionation of CO to CO_2 and C (Reaction 5).

$$2CO(g) \rightarrow CO_2(g) + C(s) \quad \text{(R5)}$$

Dollimore and Griffiths (1970) studied the decomposition of a range of oxalates under N_2 and then flowed O_2 over the pyrolysis products. A reaction between O_2 and CO was catalyzed at the solid product surfaces and for those oxalates whose solid pyrolysis products were capable of undergoing further oxidation, oxidation of the metal or lower oxide residues occurred (e.g., Fe oxalate residues consisted of Fe_2O_3 rather than Fe_3O_4). They established two groups of oxalates; those that underwent oxidation of their solid pyrolysis products upon the addition of O_2 (e.g., Fe(III), Fe(II) oxalates) and those that did not undergo oxidation of their solid pyrolysis products (e.g., Ca, Mg oxalates).

Metal acetates typically decompose to yield the metal carbonate and acetone (Reaction 6), the metal oxide, acetone, and CO_2 (Reaction 7), or the metal, C, acetic acid, CO_2, and H (Reaction 8) (Afzal et al., 1991; Bamford & Tipper, 1980; Galwey & Brown, 1999). The acetate ion can also undergo hydrolysis to form acetic acid (Reaction 9) (Wanjun & Donghua, 2007). In contrast to oxalates, major CO evolutions are not reported in acetate pyrolysis studies (Bamford & Tipper, 1980; Galwey & Brown, 1999).

$$M(CH_3COO)_2(s) \rightarrow MCO_3(s) + (CH_3)_2CO(g) \quad \text{(R6)}$$

$$M(CH_3COO)_2(s) \rightarrow MO(s) + (CH_3)_2CO(g) + CO_2(g) \quad \text{(R7)}$$

$$2M(CH_3COO)(s) \rightarrow 2M(s) + C(s) + CH_3COOH(g) + CO_2(g) + H_2(g) \quad \text{(R8)}$$

$$CH_3COO^-(s) + H_2O(g) \rightarrow CH_3COOH(g) + OH^-(g) \quad \text{(R9)}$$

Fe(II) acetate decomposes to an Fe oxide between 260 °C and 328 °C (de Souza et al., 2017). Benner et al. (2000) reported the generation of CO_2, acetone, acetic acid, and acetic anhydride from Fe(II) acetate decomposition. Ca acetate decomposes to a carbonate at ~440 °C, which is accompanied by the evolution of acetone and CO_2 (Galwey & Brown, 1999). Mg acetate decomposes between 275 °C and 340 °C to form acetone, CO_2, and MgO (Afzal et al., 1991; McAdie & Jervis, 1970). In the presence of O_2, the decomposition of acetates usually involves fewer intermediate stages and occurs at slightly different temperatures, for example, Mg acetate experiences highly exothermic decomposition between 335 °C and 351 °C under O_2 (McAdie & Jervis, 1970).

If organic salts were present in a Martian target sampled by thermal extraction, oxalates would be expected to contribute CO_2 and CO, while acetates would likely evolve a mixture of CO_2, acetone, and acetic acid. In the case of the CO_2 detections by the twin Viking Landers, a lack of indigenous acetone and acetic acid in Viking pyrolysis data was used by Benner et al. (2000) to rule out the presence of acetates in the regolith of the Viking landing sites, but CO_2 evolutions from oxalates could not be discounted. Biemann et al. (1977)

attributed the Viking CO_2 detections to desorption from mineral surfaces and carbonate decomposition. The CO_2 peaks in pyrolysis data from the 2008 Phoenix Lander were also described as consistent with the decomposition of carbonates, with supporting evidence from the lander's Microscopy, Electrochemical, and Conductivity Analyzer (MECA) instrument (Boynton et al., 2009; Sutter et al., 2012). CO_2 releases detected during SAM evolved gas analysis (EGA) experiments were attributed to background and Martian sources (Sutter et al., 2017). Potential Martian sources include atmospherically adsorbed CO_2, the decomposition of carbonates, oxidation of organic matter, decarboxylation, decarbonylation, magmatic carbon, and releases from organic matter trapped within minerals (Archer et al., 2014; Eigenbrode et al., 2014, 2018; Franz et al., 2020; Leshin et al., 2013; McAdam, Sutter, Archer, Franz, Wong, et al., 2020; Ming et al., 2014; Steele et al., 2012, 2016, 2018; Stern et al., 2018; Sutter et al., 2017). Background sources were predominantly attributed to oxidation of derivatization reagents leaked from a cup dedicated to a SAM wet chemistry experiments (Glavin et al., 2013; Leshin et al., 2013). Quantitative data analysis indicated Martian sources were responsible for a large portion of the detected CO_2 in samples (Eigenbrode et al., 2018; Franz et al., 2020; Freissinet et al., 2015, 2020; Leshin et al., 2013; Sutter et al., 2017). SAM CO was mostly coincident with at least one of the SAM CO_2 peaks and was always less than the associated CO_2 (Sutter et al., 2017). SAM CO peaks have been described as consistent with incomplete combustion of organics, the decarbonylation or decomposition of oxygen-bearing organics, and contributions from the SAM background (Eigenbrode et al., 2014; Ming et al., 2014; Sutter et al., 2017). SAM O_2 and chloromethane releases were suggestive of the presence of oxychlorine phases, such as perchlorates and chlorates, but SAM O_2 peak temperatures were below the laboratory decomposition temperatures of expected phases such as Ca and Mg perchlorates (Glavin et al., 2013; Sutter et al., 2017). Here we assess organic salts as possible sources for CO_2 and CO peaks observed in SAM EGA data. We have pyrolyzed a range of oxalate and acetate standards as pure phases, as trace phases in a silica matrix, and in mixtures with Ca and Mg perchlorate salts. Our data and conclusions inform our understanding of an important aspect of the nature of Mars' near-surface organic record and have implications for past, present, and future flight experiments.

2. Materials and Methods

2.1. Laboratory Materials

The organic salts and perchlorates used in this work were sourced commercially. Fe(III) oxalate hexahydrate, Fe(II) oxalate dihydrate, anhydrous Ca oxalate, Mg acetate tetrahydrate, Ca acetate hydrate, anhydrous Fe(II) acetate, Ca perchlorate tetrahydrate, and Mg perchlorate hexahydrate were Sigma Aldrich reagents. Mg oxalate dihydrate was sourced from MP Biomedicals, LLC.

The pyrolysis system described in Section 2.2 includes a pyrolysis oven with a quartz liner that can be etched by chlorine. To protect the liner, the organic-salt-perchlorate mixtures were dispersed in an inert matrix prior to EGA. This dispersal enabled many different mixtures to be investigated, but somewhat increased the standard error when quantifying CO_2 production from the silica-hosted samples. The inert matrix selected was the amorphous FS-120 porous ceramic silica manufactured by H.P. Technical Ceramics. FS-120 was chosen due to its high purity and porosity, which are well characterized due to FS-120's use in the MSL organic check material (Conrad et al., 2012). The FS-120 was cleaned by baking in a 550 °C oven overnight and subsamples were pyrolyzed to characterize any residual carbon contamination. The organic salt standards were dispersed in FS-120 at a 100:1 mixing ratio via grinding in a solvent-cleaned agate pestle and mortar for 3 min. In order to quantify the uncertainty introduced by this mixing, each silica mixture was analyzed in triplicate by EGA. The fused silica mixtures are likely more relevant to Martian interpretations compared to the pure organic standards, as Martian organic salts, if present, would likely occur as trace components in matrices with significant concentrations of amorphous phases (Rampe et al., 2020). The Ca and Mg perchlorate standards were added to vials of known mass that were dried down in a 60 °C oven prior to weighing. The standards were then dissolved in deionized water to form 0.04 M stock solutions.

In preparation for EGA, the samples were weighed out in Frontier Lab stainless steel Eco-Cups that had been cleaned by baking in a 550 °C oven for three hours. To examine the decomposition of the pure organic salts, 1 mg of each crystalline standard was prepared. To explore the impact of the silica on the thermal decomposition of the organic salts, 3 × 7 mg aliquots of each fused-silica-organic-salt (FSO) mixture were weighed out. To characterize the thermal decomposition of the perchlorates, the perchlorate stock solutions

were added to Eco-Cups containing fused silica at a 100:1 silica-perchlorate mixing ratio. In addition, the Ca perchlorate stock solution was added directly to an Eco-Cup so that the influence of the fused silica on perchlorate decomposition could be deconvolved. The Ca-perchlorate stock solution was added to the FSO mixtures at two different mixing ratios, 100:1 FSO-perchlorate and 1000:1 FSO-perchlorate. While the 100:1 FSO-perchlorate mixtures used 7 mg FSO aliquots, the 1000:1 mixtures used 20 mg. Mg perchlorate was added at a 100:1 FSO-perchlorate ratio only. Immediately after addition of the perchlorate stock solutions the samples were dried down in a 60 °C oven.

2.2. Laboratory Procedures

SAM-like EGA experiments were conducted on an Agilent 5975T LTM GC/MSD (low thermal mass gas chromatograph/mass spectrometer detector) system coupled to a Frontier Laboratories 3030D multi-shot pyrolyzer fitted with an Auto-Shot Sampler AS-1020E. The gas chromatograph was bypassed, and the inlet was directly connected to the MSD via an uncoated EGA column (Frontier Laboratories deactivated Ultra Alloy UADTM-2.5N column, 0.15 mm id, 2.5 m length) in the isothermal oven. In order to match the SAM flight model EGA parameters used on Mars, the inlet, column, and MSD transfer line were maintained at 135 °C and the pyrolysis oven, inlet, and column were He purged at 30 mbar. The split flow ratio to the MSD was 100:1. The pyrolysis oven was held at 50 °C when not running an experiment.

In a standard EGA run, the Auto-Shot Sampler dropped the stainless-steel cup containing the sample into the pyrolysis oven, which heated to 75 °C in 43 s and sat isothermally for 30.7 min in order to release adsorbed volatiles. This desorption temperature was slightly elevated relative to SAM initial temperatures (Glavin et al., 2013), due to the greater concentrations of water in Earth's atmosphere. The sample was then heated to 850 °C at a ramp rate of 35 °C/min and held for 6 min. Two blank runs were carried out between each analytical run to monitor the instrument background. The major differences between the SAM-like EGA experiments conducted on our commercial instrument and those carried out by the SAM flight model include the He pressure (30 mbar vs. 25 mbar), flow rate (50 sccm vs. 0.8 sccm), split flow (100:1 vs. ~800:1), and sample cup material (stainless steel vs. quartz) (Glavin et al., 2013; Mahaffy et al., 2012). As a result of these differences, variations in the relative abundances of some pyrolysis products, particularly those formed by side reactions, between our instrument and the SAM flight model are possible (Glavin et al., 2013). In addition, our commercial mass spectrometer received a greater quantity of the analyte compared to SAM due to the different split flows (Glavin et al., 2013).

SAM-like gas chromatography mass spectrometry (GC-MS) experiments were conducted on a trace 1310 GC coupled to an ISQ quadrupole mass spectrometer, both from the ThermoFisher company, in order to deconvolve some of the acetate EGA results. The GC was equipped with a Rt-Q-Bond column in fused silica (30 m long × 0.25 mm ID bonded with a 8 μm thick stationary phase) or with a metal MXT-5 column (30 m long × 0.25 mm ID bonded with a 0.25 μm thick stationary phase), both from the Restek company, for the analysis of pure Mg acetate and a fused-silica-Mg-acetate-Ca-perchlorate mixture respectively (Figure S1). Samples were analyzed using a Frontier Laboratories 3030D multi-shot pyrolyzer (Quantum Analytics) at a SAM-like pyrolysis ramp rate of 35 °C/min. Mg acetate was analyzed at two temperature ranges: 40 °C–300 °C and 300 °C–500 °C. The fused-silica-Mg-acetate-Ca-perchlorate mixture was analyzed at three temperatures ranges: 40 °C–300 °C, 300 °C–450 °C, and 450 °C–850 °C. The interface temperature between the pyrolyzer and the chromatograph varied from 140 °C to 300 °C depending on the pyrolysis temperature. During each pyrolysis step, the gaseous molecules released by the samples were trapped at the column inlet using a liquid nitrogen cold trap. Upon completion of a pyrolysis step, the cold trap was stopped, and the chromatographic analysis was started. The temperature programs used for the Rt-Q Bond column were a 35 °C hold for 5 min followed by a 10 °C/min ramp up to a final temperature of 250 °C (held for 1 min) for the temperature range 40 °C–300 °C and 270 °C (held for 1 min) for the temperature range 300 °C–500 °C. The temperature program used for the MXT-5 column was a 35 °C hold for 5 min and then a ramp up to 300 °C at a 10 °C/min rate and a hold for 1 min to bake out the column. Helium was used as the carrier gas and set at 1.2 mL/min flow rate with a split flow of 10 mL/min. The ion source and transfer line of the MS were both set at 300 °C and ions produced by electron impacts of 70 eV were scanned between mass-to-charge ratios (m/z) of 5 and 535 using a scan time of 0.2 s.

2.3. Laboratory Data Analysis

Each EGA plot was deadtime and background corrected. Deadtime correction accounts for lost counts during high count rates (Franz et al., 2014). The instrument background was calculated from the *m/z* values detected while the oven and sample sat isothermally at 75 °C. The plots were smoothed using Igor Pro's box smoothing function with an 11-point moving average. After this processing, negative values were set to zero.

The mass fragments generated by mass spectrometry of CO_2 include *m/z* 28 (CO). Therefore, when analyzing EGA data from samples that evolve both CO_2 and CO, the CO signal must be corrected for the CO fragment from CO_2. The peak area of the CO fragment was subtracted from the uncorrected *m/z* 28 peak area ($m/z\,28_{uc}$) using Equation 1 (Sutter et al., 2017), with the correction calculated from laboratory EGA of a calcite standard where no CO producers were present.

$$m/z\,28_c = m/z\,28_{uc} - (m/z\,44 \times (m/z\,28/m/z\,44)_{calcite}) \quad \text{(E1)}$$

The species reported during SAM-like pyrolysis-GC-MS of the Mg acetate standard included CO_2, methane, ethane, ethene, propane, propene, acetaldehyde, methyl-propane, methyl-propene, acetone, acetic acid, butanone, butenone, and pentanone (Table S1). These species were inferred to be predominantly acetate pyrolysis products rather than impurities as the Mg acetate standard had >99% purity and side reactions during acetate pyrolysis are reported in the literature (McAdie & Jervis, 1970). Benner et al. (2000) reported the detection of acetic anhydride during pyrolysis of Fe(II) acetate in addition to acetone and acetic acid. Many of the species listed in Table S1 produce *m/z* 44 fragments (e.g., CO_2, C_2H_4O, C_3H_8) and *m/z* 28 fragments (e.g., CO, C_2H_4) during mass spectrometry, which has significant implications for interpretations about CO_2 and CO in our acetate EGA data. CO_2 was assumed to be the only contributor to *m/z* 22 (as CO_2^{2+}), so the *m/z* 22 profile was used to assess what proportion of the *m/z* 44 profile was sourced from CO_2 (Equation 2).

$$m/z\,44_{CO_2} = m/z\,22_{sample} \times ((m/z\,44/m/z\,m/z\,22)_{calcite}) \quad \text{(E2)}$$

Acetate *m/z* 28 peaks were corrected for the CO fragment from CO_2 but not for contributions from the organic products of acetate pyrolysis. The EGA profiles of acetone and acetic acid were used to infer how significant the contribution of organic fragments to $m/z\,28_c$ were.

Areas under the curve were calculated for *m/z* 44 in Igor Pro and converted to masses using a CO_2 calibration curve constructed using the CO_2 evolutions from known masses of calcite. The *m/z* 18 (H_2O) peaks produced by the pure organic salts during EGA were used to determine if the hydration state of the salts differed from the description on the sample bottle. The mass of the water of hydration was subtracted from the weighed masses in order to determine the CO_2 release from the anhydrous salts. Each organic-salt-fused-silica mixture was run in triplicate to quantify the standard error introduced by sample mixing. This error was combined with the standard error of the calibration curve and the mass balance error. The total peak area for the corrected *m/z* 28 peaks detected during EGA of each oxalate sample were measured and ratioed to the total peak area for *m/z* 44 peaks in order to examine how CO/CO_2 ratios changed upon mixing oxalates in fused silica and mixing the silica-oxalate mixtures with perchlorates. This was not calculated for acetates due to the large number of acetate pyrolysis products that can contribute to *m/z* 28.

2.4. Geologic Context of SAM Samples

The Martian materials examined by SAM include modern eolian deposits sampled at three separate localities (Leshin et al., 2013; Stern et al., 2018; Sutter et al., 2017). Rocknest (RN) was acquired from an inactive sand shadow composed of unconsolidated sand and dust that represented a mixture of local, regional, and global sources (Blake et al., 2013; Minitti et al., 2013; Stern et al., 2018; Sutter et al., 2017). Gobabeb (GB) and Ogunquit Beach (OG) were obtained from an active eolian dune field on the flanks of Aeolian Mons (informally known as Mount Sharp) that lacked silt and dust-sized grains and likely represented a regional source (Stern et al., 2018).

The first drilled samples analyzed by SAM were from the Sheepbed mudstone within the Yellowknife Bay formation (Figure S2; Table S2), which represented an ancient circumneutral lake environment ideal for the preservation of organic matter (Eigenbrode et al., 2018; Grotzinger et al., 2014; Sutter et al., 2017).

The John Klein (JK) drill hole was intersected by light-toned millimeter-sized veins that likely indicated post-depositional diagenesis by groundwater, while Cumberland (CB) exhibited far fewer veins (Eigenbrode et al., 2018; Sutter et al., 2017; Vaniman et al., 2014). MSL's next drill target was Windjana (WJ), a cross-stratified eolian sandstone from the Kimberley formation that consisted of reworked fluvial grains from multiple parent rock sources (Sutter et al., 2017; Treiman et al., 2016).

The Confidence Hills (CH), Mojave (MJ), and Telegraph Peak (TP) targets were the first located within the Murray formation (the basal layer of the Mount Sharp Group) and were found to be complex mixtures where phases stable under acidic, alkaline, oxidizing, and reducing conditions were present (Rampe et al., 2017; Sutter et al., 2017). Diagenetic features were observed close to the CH and MJ drill sites and the TP target had elevated Si (Nachon et al., 2017; Sutter et al., 2017). Buckskin (BK) was drilled from a finely laminated mudstone 6 m stratigraphically above TP and was also found to have high Si (Morris et al., 2016; Sutter et al., 2017).

Big Sky (BY) and Greenhorn (GH) were drilled from the Stimson formation, a cross-bedded eolian sandstone that uncomformably overlies the Murray (Fraeman et al., 2016; Sutter et al., 2017). BY was sampled from parent rock, while GH was from an alteration halo that appeared to have been leached by fluids (Rampe et al., 2020; Sutter et al., 2017; Yen et al., 2017). Upon returning to the Murray, MSL drilled Oudam (OU) from a cross-stratified eolian and fluvial siltstone in the Hartmann's Valley member, and Marimba (MB) from a finely laminated lacustrine mudstone in the Karasburg member (Bristow et al., 2018).

After recovering from a drill fault, MSL examined Vera Rubin Ridge (VRR), an erosion-resistant feature with widespread evidence for diagenesis (Fraeman et al., 2013, 2020; McAdam, Sutter, Archer, Franz, Wong, et al., 2020). The VRR was divided into the Pettegrove Point member, which was composed of finely laminated mudstones, and the Jura member, which consisted of finely laminated mudstones to fine sandstones, with red and gray color variations (Fraeman et al., 2020; McAdam, Sutter, Archer, Franz, Wong, et al., 2020). Duluth (DU) was drilled directly beneath the VRR, Stoer (ST) from the Pettegrove Point member, Highfield (HF) from the gray Jura, and Rock Hall (RH) from the red Jura (McAdam, Sutter, Archer, Franz, Wong, et al., 2020).

In 2019, MSL began exploring the Glen Torridon (GT) region, which featured strata strongly associated with smectite clay mineral spectra that were subdivided into smooth, fractured, and fractured intermediate clay-bearing units (V. K. Fox et al., 2020; Grotzinger et al., 2012; Thorpe et al., 2020). Kilmarie (KM) was drilled from the smooth clay-bearing unit in the Jura and Glen Etive (GE) from the fractured clay-bearing unit in the Knockfarril Hill member, a cross-laminated sandstone (Sutter, McAdam, Achilles, et al., 2020; Thorpe et al., 2020). Hutton (HU) was sampled close to an unconformity between the fractured intermediate unit and the overlying Greenheugh Pediment (Bryk et al., 2020; McAdam, Sutter, Archer, Franz, Eigenbrode, et al., 2020). MSL climbed the pediment and acquired the Edinburgh (EB) sample from the cross-bedded sandstone capping unit, which was interpreted to be part of the Stimson formation (Bryk et al., 2020; Sutter, McAdam, Archer, et al., 2020). MSL descended off the pediment and drilled Glasgow (GG) from the fractured intermediate unit and Mary Anning (MA) from the Knockfarril Hill member.

2.5. SAM Data Analysis

The quantities of CO_2 evolved by organic salts in our experiments were compared to the abundances of CO_2 evolved by SAM samples in order to set upper limits on organic salt concentrations within Gale crater. SAM CO_2 and O_2 abundances and uncertainties were calculated based on a SAM analysis of an equimolar mixture of gas containing O_2, CO_2, N_2, and Ar and SAM EGA of known masses of calcite prior to launch (Archer et al., 2014). SAM CO_2 was corrected for the maximum potential contribution from leaking SAM derivatization agents of 900 nmol C for each SAM-EGA experiment (Sutter et al., 2017).

The SAM detector is tuned to detect trace species, so abundant gases such as CO_2 can saturate the detector (Archer et al., 2014). When plotting SAM CO_2 data, missing portions of the m/z 44 peak were replaced with the corrected isotopologue m/z 45 ($^{13}CO_2$) (Sutter et al., 2017). The m/z 45 fragment was used to infer SAM CO_2 rather than m/z 22 as the m/z 45 fragment from CO_2 is more intense than the m/z 22 fragment in SAM mass spectrometry. SAM m/z 28 peaks were corrected for contributions from the CO fragment from CO_2, ethane, and formaldehyde using Equation 3 (McAdam, Sutter, Archer, Franz, Wong, et al., 2020).

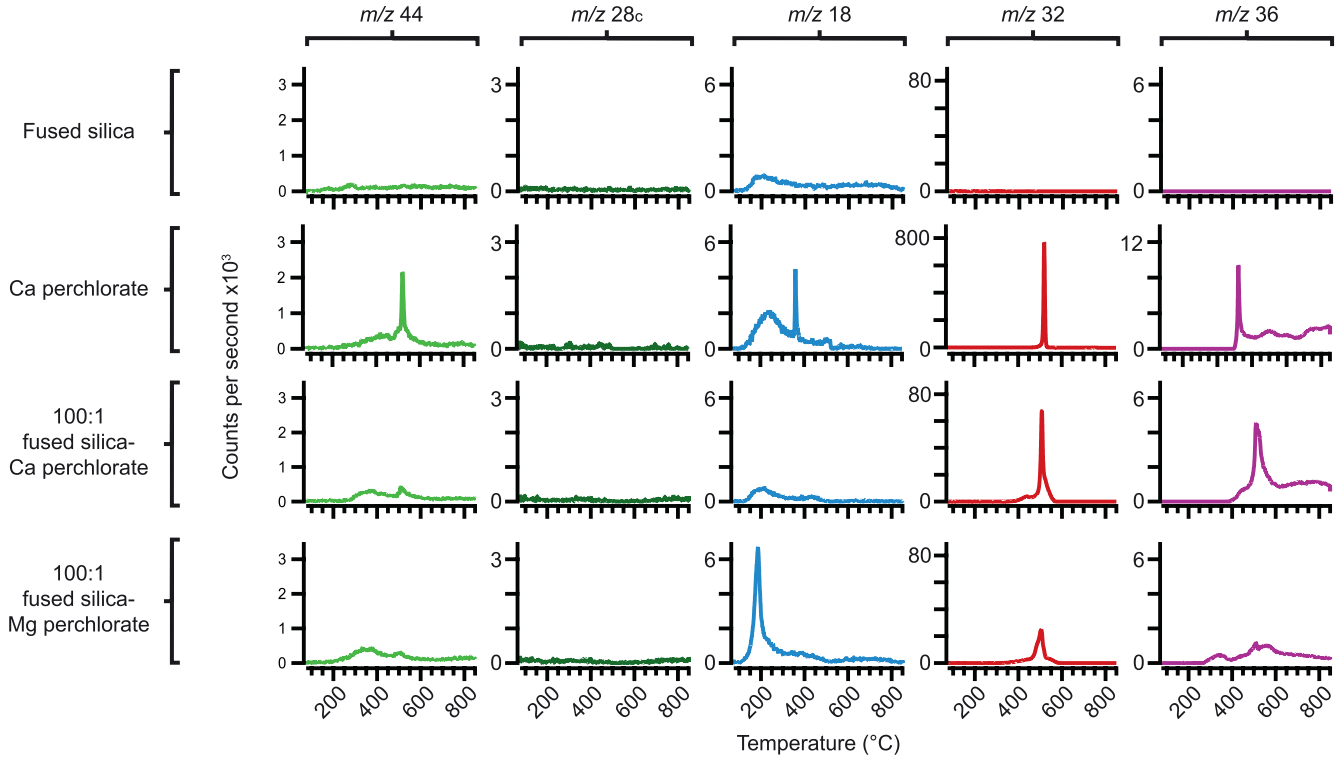

Figure 1. Evolved m/z 44 (CO_2), m/z 28_c (corrected CO), m/z 18 (H_2O), m/z 32 (O_2), and m/z 36 (HCl) versus temperature as detected by SAM-like EGA of the FS-120 fused silica, Ca perchlorate, a 100:1 fused-silica-Ca-perchlorate mixture, and a 100:1 fused-silica-Mg-perchlorate mixture. EGA, evolved gas analysis; SAM, Sample Analysis at Mars.

$$\text{SAM CO} = m/z\,28 - m/z\,45 \times 3.20 - m/z\,27 \times 3 - m/z\,29 \times 0.24 \quad \text{(E3)}$$

SAM CO_2 and CO were plotted against modeled sample temperature. SAM has two pyrolysis ovens, oven-1, which has an external temperature sensor, and oven-2, which has a secondary heater wire in place of a temperature sensor (Franz et al., 2020). As the mission has progressed the temperature model for samples analyzed in oven-2 has been refined and in this work the oven-2_model-2 estimation described in Franz et al. (2020) is used for oven-2 samples.

MSL's drill fault prior to exploration of the VRR required transitioning to a new drilling method known as feed-extended sample transfer (FEST) (Fraeman et al., 2020). FEST ensured that drilled samples could still be acquired but MSL's Collection and Handling for Interior Martian Rock Analysis (CHIMRA) system could no longer be used, which resulted in a larger uncertainty in delivered sample mass (McAdam, Sutter, Archer, Franz, Wong, et al., 2020).

3. Results

3.1. Pyrolysis of Fused Silica and Perchlorates

The FS-120 fused silica evolved a broad H_2O peak at 205 °C and a very weak CO_2 peak at 280 °C during SAM-like EGA, with H_2O and CO_2 remaining slightly elevated for the rest of the run (Figure 1). No O_2 or HCl peaks were produced by the fused silica. Ca perchlorate evolved sharp O_2, HCl, Cl_2, and CO_2 peaks at 520 °C as the Ca perchlorate decomposed to form $CaCl_2$. The HCl and Cl_2 releases were unexpected as perchlorates that decompose into chlorides are reported in the literature as evolving O_2 only (Marvin & Woolaver, 1945). It is theorized that as the perchlorate began to decompose, some hydrolysis may have occurred or that the evolved O_2 may have reacted with residual perchlorate to form CaO and perchloric acid, with residual H_2O in the system acting as the source of hydrogen. The H_2O profile featured peaks at 240 °C and 360 °C and a sharp drop at 520 °C as the perchlorate decomposed. A broad high-temperature HCl release

(starting at ~600 °C) occurred due to the $CaCl_2$ residue melting and reacting with H_2O (Clark et al., 2020; Sutter et al., 2017). An additional small CO_2 peak was detected at ~420 °C. The CO_2 peaks shown in Figure 1 likely originated from carbon contamination in the fused silica and the perchlorate standards. The amounts of CO_2 produced by the silica and perchlorates were significantly less than those detected during pyrolysis of the organic salts (Table S3).

The 100:1 fused-silica-Ca-perchlorate mixture evolved broad O_2 and HCl peaks at 505 °C. The H_2O profile below 500 °C was similar to that of the fused-silica experiment and somewhat similar to the Ca-perchlorate run. The elevated H_2O seen at high temperatures in the fused-silica run was absent in this experiment. A broad CO_2 peak was observed at 370 °C and a small sharp CO_2 peak was detected at 505 °C. The 100:1 fused-silica-Mg-perchlorate mixture also evolved O_2 and HCl peaks at 505 °C, but HCl began to evolve at significantly lower temperatures (starting at ~265 °C) and the 505 °C HCl and O_2 peaks were weaker. Mg perchlorate predominantly decomposes to form an oxide residue and Cl_2 gas (Marvin & Woolaver, 1945; Sutter et al., 2017). However, Cl_2 was not detected during either silica-perchlorate run, indicating it was fully converted to HCl as the Cl_2 diffused out of the fused silica matrix, with hydrogen supplied by hydroxyl groups adsorbed to the silica and residual H_2O. The high-temperature HCl seen in the Mg perchlorate experiment suggested that some $MgCl_2$ formed as Mg perchlorate decomposed, which has been observed in the literature by Steininger et al. (2012). Mg perchlorate evolved a sharp H_2O peak at 200 °C. Small CO_2 peaks were detected at 350 °C and 505 °C.

3.2. Pyrolysis of Oxalates and Oxalate-Perchlorate Mixtures

The oxalate standards evolved CO_2 over a wide temperature range during SAM-like EGA. The lowest temperature release was from Fe(III) oxalate, which began to produce CO_2 from 160 °C. The highest temperature release was from Ca oxalate, which evolved CO_2 as two discrete peaks, with decomposition of the $CaCO_3$ intermediate continuing up to 770 °C. The majority of CO_2 peaks produced by oxalate pyrolysis were accompanied by strong releases of CO, as expected for decomposition reactions involving the formation of carbonates or oxides, as shown in Reactions 1 and 2 in Section 1. Fe oxalate CO_2 and CO evolutions were significantly affected by the presence of perchlorates, while Ca and Mg oxalates were resistant to peak shifting.

3.2.1. Pyrolysis of Fe(III) Oxalate

Pure Fe(III) oxalate evolved CO_2 peaks at 210 °C and 400 °C during SAM-like EGA (Figure 2), which was consistent with the formation and decomposition of an Fe(II) oxalate intermediate, as shown in Reactions 2 and 4 in Section 1. The 400 °C CO_2 peak was accompanied by a sharp CO release while the 210 °C peak had no associated CO, indicating that the transformation of Fe(III) oxalate to Fe(II) oxalate was highly efficient.

The EGA profile of the 100:1 fused-silica-Fe(III)-oxalate mixture (FSFeIIIOx) was largely unchanged from that of the pure oxalate. The 1000:1 FSFeIIIOx-Ca-perchlorate mixture exhibited broadening of its low-temperature CO_2 peak. In addition, the second CO_2 release weakened and shifted to 375 °C and was part of a large shoulder that extended up to 450 °C, with both the 375 °C peak and the shoulder tracked by CO. The 100:1 FSFeIIIOx-perchlorate mixtures produced broad CO_2 peaks at ~220 °C, which exhibited shoulders that extended up to ~370 °C. No 400 °C CO_2 peaks were produced by the 100:1 FSFeIIIOx-perchlorate runs, and no CO peaks were detected. The CO was likely completely oxidized to CO_2.

H_2O peaks were detected between ~150 °C and 200 °C in each experiment as the silica, Fe(III) oxalate, and perchlorate salts dehydrated. No O_2 was detected in the 1000:1 FSFeIIIOx-Ca-perchlorate run, which suggests the O_2 was completely consumed by oxidation reactions. O_2 was detected in the 100:1 FSFeIIIOx-perchlorate runs but only as weak releases peaking between 420 °C and 450 °C. The onset of the major O_2 evolution from Ca perchlorate began at a slightly lower temperature than in the Ca-perchlorate-only experiment (Figure 1).

The HCl peak produced by the fused-silica-Ca-perchlorate run at 505 °C was not detected in the presence of Fe(III) oxalate. Because Fe(III) oxalate consumes O_2 as it decomposes, the non-detection of mid-temperature HCl supports the hypothesis that O_2 played a role in in the formation of the 505 °C HCl peak in the fused-silica-Ca-perchlorate run. Each perchlorate mixture produced a high temperature HCl peak as the melting chloride residues reacted with H_2O (Clark et al., 2020; Sutter et al., 2017). A small HCl peak was

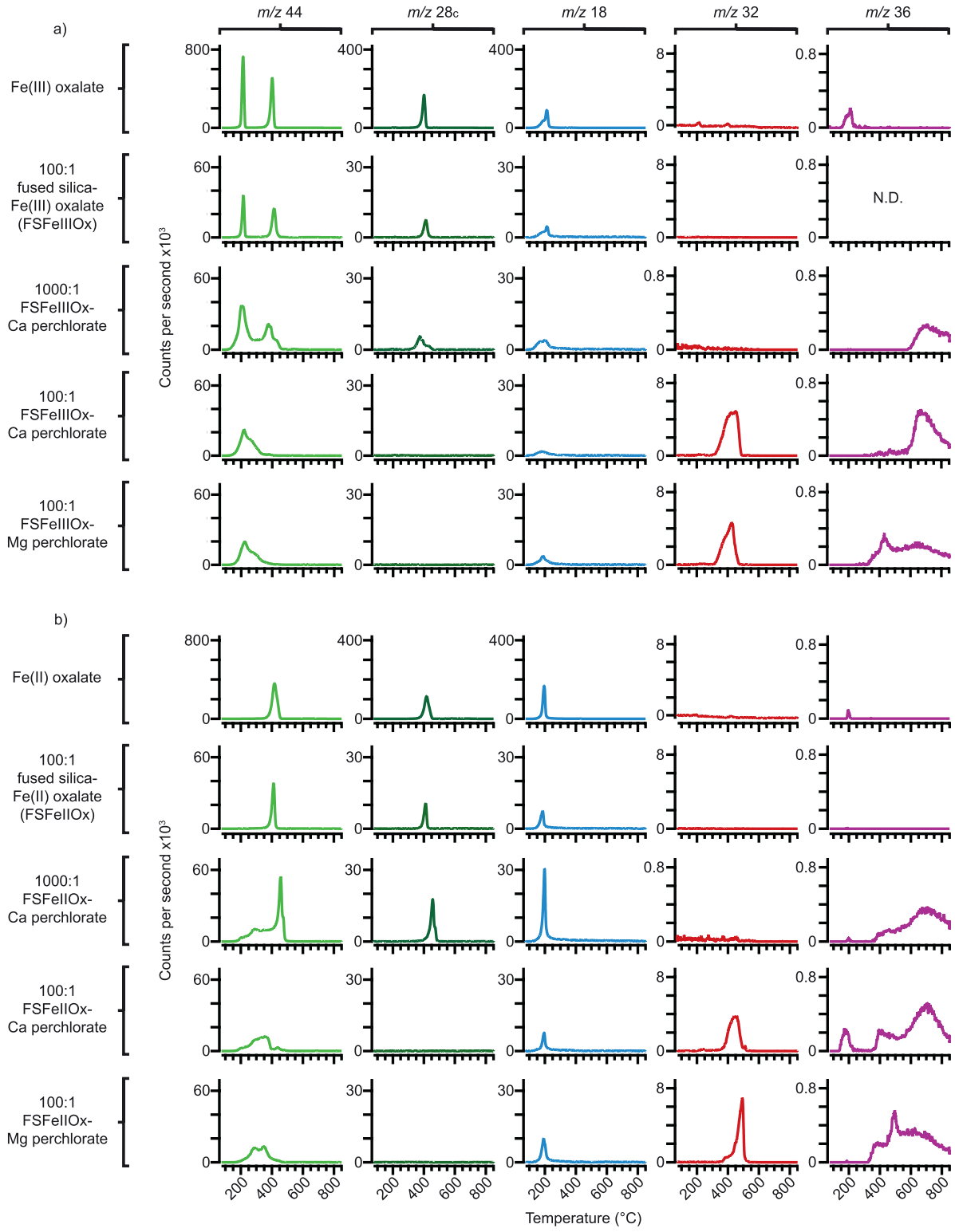

Figure 2. Evolved m/z 44 (CO_2), m/z 28_c (corrected CO), m/z 18 (H_2O), m/z 32 (O_2), and m/z 36 (HCl) versus temperature as detected by SAM-like EGA of (a) Fe(III) oxalate and (b) Fe(II) oxalate as pure phases, as FSFeOx, as 1000:1 FSFeOx and Ca perchlorate mixtures, as 100:1 FSFeOx and Ca perchlorate mixtures, and as 100:1 FSFeOx and Mg perchlorate mixtures. N.D. stands for no detection, which indicates that no signal was detected for m/z 36 during EGA of the FSFeIIIOx mixture. It should be noted that 1 mg aliquots were used for the pure oxalate experiments, 7 mg aliquots for the 100:1 silica and silica-perchlorate mixtures, and 20 mg aliquots for the 1000:1 mixtures. EGA, evolved gas analysis; FSFeOx, 100:1 mixtures of fused silica and Fe oxalate.

detected at 200 °C in the pure Fe(III) oxalate run, which likely originated from H_2O reacting with minor amounts of Cl contamination present in the quartz liner of the pyrolysis oven. This background Cl is usually removed by the blank runs, but it can persist for longer if particularly Cl-rich samples have been run or if the liner is nearing the end of its lifetime. The pure organic salt samples were the last set of samples analyzed in this project, so the chance of background Cl was somewhat greater.

3.2.2. Pyrolysis of Fe(II) Oxalate

Pure Fe(II) oxalate evolved CO_2 and CO peaks at 418 °C during SAM-like EGA (Figure 2). These peaks became sharper in the 100:1 fused-silica-Fe(II)-oxalate (FSFeIIOx) run. The CO_2 profile of the 1000:1 FSFeIIOx-Ca-perchlorate sample featured a prominent low-temperature shoulder that evolved from 175 °C. CO was detected, but only with a sharp CO_2 peak at 455 °C, which was indicative of standard Fe(II) oxalate decomposition via Reaction 2 in Section 1, while the low-temperature CO_2 shoulder indicated that some of the Fe(II) oxalate decomposed via a different reaction, which likely involved O_2 sourced from Ca perchlorate. It was unexpected for Fe(II) oxalate and Ca perchlorate to begin decomposing at such low temperatures. The oxidative decomposition of Fe(II) oxalate is known to be accompanied by a local sample temperature increase related to intense oxidation as the oxidation state of Fe increases (Hermankova et al., 2010). If the presence of Fe(II) oxalate lowered the decomposition temperature of Ca perchlorate, the earlier onset of O_2 evolution and the resulting local temperature increase may have enhanced decomposition of both the oxalate and the perchlorate.

The 100:1 FSFeIIOx-perchlorate runs produced broad CO_2 peaks between 200 °C and 400 °C, with the most prominent evolutions occurring at 280 °C and 350 °C. The 350 °C peak coincided with the onset of the major O_2 and HCl releases. Between 400 °C and 450 °C a minor CO_2 peak was detected in the Ca-perchlorate mixture and a minor CO_2 shoulder was evolved by the Mg-perchlorate mixture. These features occurred at similar temperatures to the sharp 455 °C CO_2 peak evolved by the 1000:1 mixture, which suggests that at greater perchlorate concentrations, only broad low-temperature CO_2 peaks would be evolved.

As with the Fe(III) oxalate experiments, sharp H_2O peaks occurred between ~150 °C and 200 °C as the mixtures dehydrated. Similarly, the O_2 from Ca perchlorate was entirely consumed by oxidation reactions in the 1000:1 FSFeIIOx-Ca-perchlorate experiment. The 100:1 FSFeIIOx-Ca-perchlorate run evolved a minor O_2 peak at ~450 °C, while the Mg perchlorate mixture produced a weak O_2 peak at ~500 °C, which was consistent with the peak temperature of the Mg-perchlorate-only run. The perchlorate-bearing samples produced mid-temperature HCl evolutions that were more prominent than those evolved by the Fe(III) oxalate mixtures. Low-temperature HCl peaks were evolved by the pure Fe(II) oxalate standard and the perchlorate mixtures. The HCl peak in the pure oxalate run was likely due to Cl in the oven liner reacting with H_2O. It is possible that this Cl source also contributed in the perchlorate runs, but the FSFeIIOx-perchlorate mixtures were the only perchlorate mixtures that demonstrated this behavior. It is also possible that the abundant O_2 and Fe^{2+} in these runs led to highly exothermic conditions that enabled some hydrolysis of the perchlorate to occur.

3.2.3. Pyrolysis of Ca Oxalate

Pure Ca oxalate evolved CO and CO_2 peaks at 535 °C (with CO producing the more prominent peak) as the oxalate decomposed to form $CaCO_3$ (Figure 3). The co-evolution of CO and CO_2 suggests that some disproportionation of the CO occurred to form CO_2 and C (Reaction 5 in Section 1). It is also possible that some of the CO was oxidized by background O_2 in the instrument. The $CaCO_3$ residue began to evolve CO_2 from 590 °C and formed a peak at 730 °C. The 100:1 fused-silica-Ca-oxalate mixture (FSCaOx), produced a slightly weaker CO release and the CO_2 peak evolved by decomposition of the $CaCO_3$ intermediate weakened and shifted ~80 °C lower.

The CO_2 and CO peaks evolved by Ca oxalate decomposition did not shift significantly when minor concentrations of Ca perchlorate were added to the silica mixture (1000:1 FSCaOx-Ca-perchlorate). However, the 535 °C CO_2 peak did strengthen in comparison to the $CaCO_3$ CO_2 peak, which shifted to 690 °C. In the presence of elevated perchlorate concentrations (100:1 FSCaOx-perchlorate), the CO_2 release from Ca oxalate decomposition strengthened and the CO release weakened, but there was still no significant peak shifting. The CO_2 release from the $CaCO_3$ intermediate weakened and shifted 30 °C–70 °C lower. The $CaCO_3$ likely reacted with HCl and began to decompose at lower temperatures (Cannon et al., 2012).

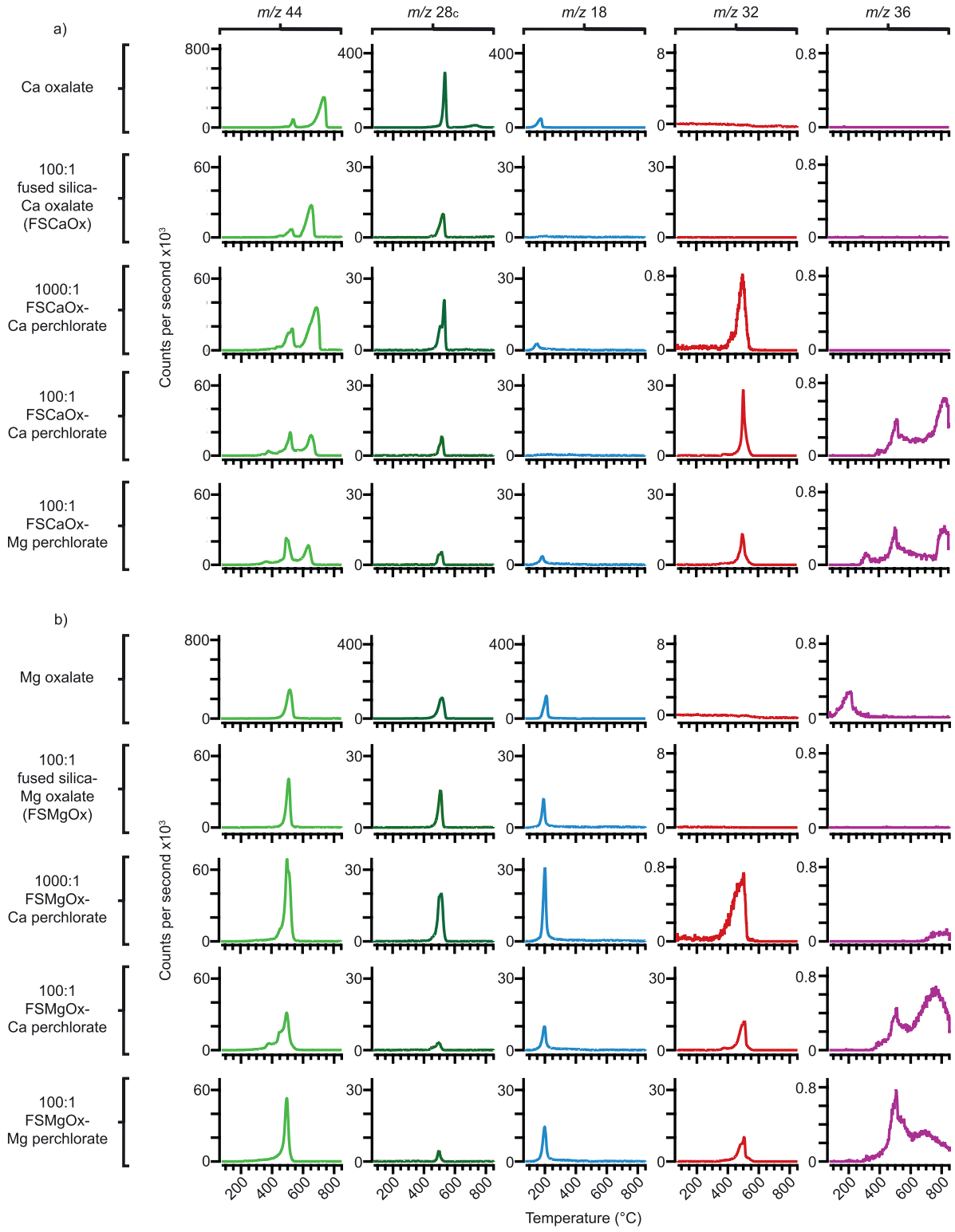

Figure 3. Evolved *m/z* 44 (CO_2), *m/z* 28_c (corrected CO), *m/z* 18 (H_2O), *m/z* 32 (O_2), and *m/z* 36 (HCl) versus temperature as detected by SAM-like EGA of (a) Ca oxalate and (b) Mg oxalate as pure phases, as FSOx, as 1000:1 FSOx and Ca perchlorate mixtures, as 100:1 FSOx and Ca perchlorate mixtures, and as 100:1 FSOx and Mg perchlorate mixtures. It should be noted that 1 mg aliquots were used for the pure oxalate experiments, 7 mg aliquots for the 100:1 silica and silica-perchlorate mixtures, and 20 mg aliquots for the 1000:1 mixtures. EGA, evolved gas analysis; FSOx, 100:1 mixtures of fused silica and oxalate; SAM, Sample Analysis at Mars.

Ca oxalate was purchased as the anhydrous form but several of the runs evolved low-temperature H_2O peaks between 100 °C and 200 °C. The peaks seen in the pure Ca oxalate run and the 1000:1 FSCaOx-Ca perchlorate run suggest that the Ca oxalate was hydrated. This hydration would be unlikely to significantly impact the decomposition of the oxalate, as dehydration and decomposition are well-separated steps.

The O_2 release temperatures from Ca and Mg perchlorate were largely unaffected by the presence of Ca oxalate. Unlike Fe oxalates, Ca oxalate does not undergo oxidation of its solid pyrolysis products (Dollimore & Griffiths, 1970). However, the weaker O_2 peaks produced by the FSCaOx-perchlorate mixtures relative to the perchlorate-only runs suggest that some O_2 was consumed by oxidation reactions with CO. The weak O_2 peak from the 1000:1 FSCaOx-Ca-perchlorate run also showed no peak shifting. Prominent high-temperature HCl evolutions were produced by the 100:1 FSCaOx-perchlorate mixtures and Ca perchlorate continued to evolve a significant 505 °C HCl peak in the presence of Ca oxalate. No HCl peaks were observed in the 1000:1 FSCaOx-Ca-perchlorate experiment, it was likely consumed by the abundant $CaCO_3$.

3.2.4. Pyrolysis of Mg Oxalate

Pure Mg Oxalate evolved CO_2 and CO peaks at 518 °C during SAM-like EGA (Figure 3). No secondary CO_2 peak was observed, consistent with the decomposition of a $MgCO_3$ intermediate, as described by Gadalla (1984). The 518 °C CO_2 peak sharpened but did not shift in the 100:1 fused-silica-Mg-oxalate mixture (FSMgOx) and the perchlorate mixtures but the 100:1 FSMgOx-Ca-perchlorate mixture developed two CO_2 shoulders at lower temperatures, which occurred with the onset of O_2 evolution from Ca perchlorate. The Mg oxalate CO peak weakened with increasing perchlorate concentrations.

Prominent H_2O releases were detected in each run at ~200 °C. As with the Ca oxalate experiments, the perchlorate O_2 peaks weakened in the presence of Mg oxalate but did not shift. A low-temperature HCl peak was detected in the pure Mg oxalate run, which was similar to those seen in the Fe oxalate experiments and inferred to be instrumental. A small HCl peak was detected at high temperatures in the 1000:1 FSMgOx-Ca perchlorate run and prominent mid- and high-temperature HCl peaks were observed in the 100:1 FSMgOx-perchlorate experiments.

3.2.5. Quantification of Oxalate CO_2 Production During Pyrolysis

In order to accurately calculate the CO_2 production from each oxalate, the different hydration states of the standards had to be accounted for. The H_2O peaks observed in Figures 2 and 3 were consistent with Fe(III) oxalate hexahydrate, Fe(II) oxalate dihydrate, and Mg oxalate dihydrate. Ca oxalate was inferred to have been in the monohydrate form rather than the anhydrous form. The mass of the water of hydration was subtracted from each standard in order to calculate the CO_2 production per mg of each anhydrous oxalate.

Pure Fe(III) oxalate produced more CO_2 during EGA compared to the other oxalates studied (Table 1; Table S4). Unlike Fe(II), Ca, and Mg oxalates, Fe(III) oxalate transforms into Fe(II) oxalate during pyrolysis, which involves a prominent release of CO_2 (Reaction 4 in Section 1). Pure Ca, Mg, and Fe(II) oxalates produced similar CO/CO_2 peak area ratios, while for Fe(III) oxalate the ratio was markedly lower. When dispersed in fused silica, Fe(III) oxalate evolved slightly less CO_2 and there was an increase in the CO/CO_2 peak area ratio, which suggests that the silica matrix inhibited oxidation of CO by background O_2. Fe(II) oxalate and Mg oxalate also showed moderate increases in their CO/CO_2 ratios. In contrast, Ca oxalate evolved significantly more CO_2 in fused silica and the CO/CO_2 ratio decreased. It is possible that in a matrix the standard decomposition of Ca oxalate to a carbonate (Reaction 1 in Section 1) was inhibited and Ca oxalate decomposition to the oxide or metal may have occurred (Reactions 2 and 3 in Section 1). This hypothesis would explain why the CO_2 peak from $CaCO_3$ decomposition was observed to weaken and shift to lower temperatures and why less CO was detected. SAM-like EGA of other carbonate-generating oxalates, such as K oxalate, exhibited similar behavior. K_2CO_3 is stable in the SAM temperature range, yet when dispersed in fused silica the amounts of CO_2 detected as K oxalate decomposed increased significantly and there was a dramatic reduction in the CO/CO_2 ratio (Table S5). This effect was likely less apparent in the Mg oxalate experiment due to the instantaneous decomposition of the $MgCO_3$ intermediate.

The CO/CO_2 peak area ratio decreased for each oxalate when minor concentrations of Ca perchlorate were added to the fused-silica-oxalate mixtures. Fe oxalate and Mg oxalate showed only minor changes in the quantities of CO_2 evolved that were within error of the fused-silica-oxalate mixtures, while the quantity

Table 1
The Quantities of CO_2 and CO/CO_2 Ratios Produced by Oxalates, Fused-Silica-Oxalate Mixtures, and Fused-Silica-Oxalate-Perchlorate Mixtures During EGA

Sample	Cation	CO_2 (μmol CO_2/mg anhydrous oxalate salt)	Total CO/CO_2 peak area ratio	Average CO_2 (μmol CO_2/mg anhydrous oxalate salt)	1σ
Pure oxalates	Fe(III)	15.24 ± 0.16	0.16	10.72 ± 0.15	3.05
	Fe(II)	8.65 ± 0.15	0.30		
	Ca	9.10 ± 0.12	0.37		
	Mg	9.90 ± 0.18	0.38		
FSOx	Fe(III)	12.40 ± 2.08	0.22	11.28 ± 2.27	2.43
	Fe(II)	7.92 ± 2.02	0.32		
	Ca	13.54 ± 1.97	0.28		
	Mg	11.27 ± 3.00	0.39		
1000:1 FSOx-Ca perchlorate	Fe(III)	13.42 ± 0.75	0.07	10.88 ± 0.81	1.70
	Fe(II)	10.10 ± 0.73	0.15		
	Ca	9.98 ± 0.70	0.18		
	Mg	10.02 ± 1.06	0.26		
100:1 FSOx-Ca perchlorate	Fe(III)	16.48 ± 2.06	–	16.28 ± 2.23	2.36
	Fe(II)	13.13 ± 2.00	–		
	Ca	16.71 ± 1.96	0.17		
	Mg	18.83 ± 2.91	0.07		
100:1 FSOx-Mg perchlorate	Fe(III)	16.21 ± 2.07	–	16.38 ± 2.30	2.07
	Fe(II)	13.67 ± 2.08	-		
	Ca	16.98 ± 2.01	0.14		
	Mg	18.65 ± 3.03	0.05		
Average oxalate CO_2 production at low perchlorate concentrations				11.08 ± 1.54	1.95
Average oxalate CO_2 production at high perchlorate concentrations				16.33 ± 2.26	2.06

Abbreviations: EGA, evolved gas analysis; FSOx, 100:1 fused-silica-oxalate mixtures.

of CO_2 produced by Ca oxalate was more in line with the pure oxalate. Each fused-silica-oxalate mixture evolved greater amounts of CO_2 at elevated perchlorate concentrations. While CO was scrubbed in the Fe oxalate mixtures, CO peaks were still observed in the Mg and Ca oxalate runs. The somewhat greater CO_2 production from Ca and Mg oxalates relative to Fe oxalates at elevated perchlorate concentrations was therefore not solely due to CO oxidation. Prominent HCl peaks were detected in each perchlorate run, which would have reacted with the carbonates to form CO_2 and chloride residues. Variations in perchlorate type did not have a substantial impact on the amounts of CO_2 generated by oxalates, which suggests that oxalate decomposition is not particularly sensitive to minor changes in O_2 concentrations during pyrolysis.

3.3. Pyrolysis of Acetates and Acetate-Perchlorate Mixtures

The majority of the acetate CO_2 releases observed during SAM-like EGA were accompanied by peaks for acetone (*m/z* 58), acetic acid (*m/z* 60), and minor *m/z* 28_c evolutions that were a mixture of CO and fragments from organic pyrolysis products (Table S1). The acetate *m/z* 44 profiles were compared to our calculated *m/z* 44_{CO2} traces, which indicated that the *m/z* 44 contributions from organic acetate pyrolysis products were minor (Figure S3). Fe(II) acetate produced the lowest-temperature CO_2 release, with the onset beginning at 190 °C. Ca acetate formed $CaCO_3$ during pyrolysis, which evolved CO_2 up to 770 °C. In contrast to the oxalates, the *m/z* 28_c evolutions for pure acetates were extremely weak relative to CO_2.

Pure Fe(II) acetate produced similar sized peaks for acetone and acetic acid during EGA, while for Ca and Mg acetate, acetone was dominant. These observations suggest that Ca and Mg acetate produced a metal

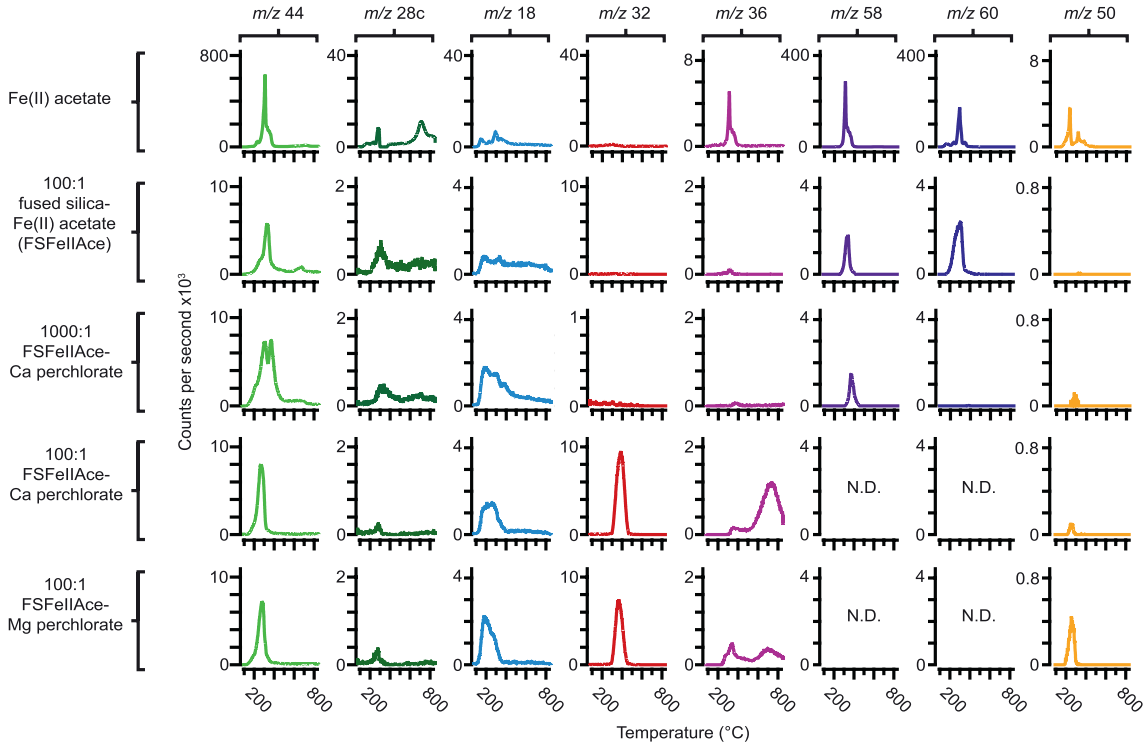

Figure 4. Evolved m/z 44 (CO_2, organic fragments), m/z 28_c (corrected CO, organic fragments), m/z 18 (H_2O, organic fragments), m/z 32 (O_2), m/z 36 (HCl, organic fragments), m/z 58 (acetone), m/z 60 (acetic acid), and m/z 50 (chloromethane, organic fragments) versus temperature as detected by SAM-like EGA of pure Fe(II) acetate, FSFeIIAce, a 1000:1 FSFeIIAce and Ca perchlorate mixture, a 100:1 FSFeIIAce and Ca perchlorate mixture, and a 100:1 FSFeIIAce and Mg perchlorate mixture. N.D. stands for no detection, which indicates that no signals were detected for m/z 58 and m/z 60 during EGA of the 100:1 perchlorate mixtures. It should be noted that a 1 mg aliquot was used for the pure acetate experiment, 7 mg aliquots for the 100:1 silica and silica-perchlorate mixtures, and a 20 mg aliquot for the 1000:1 mixture. EGA, evolved gas analysis; FSFeIIAce, a 100:1 mixture of fused silica and Fe(II) acetate; SAM, Sample Analysis at Mars.

carbonate or oxide during pyrolysis (Reactions 6 and 7 in Section 1), with minor amounts of the free metal (Reaction 8), and Fe(II) acetate produced similar proportions of the free metal and the oxide (Bamford & Tipper, 1980). Though acetone and acetic acid were the most abundant organic products, a multitude of additional minor masses were detected during EGA that were indicative of other organic species (Table S1). Methane (m/z 16) was not plotted on Figures 4–6 as several of the species listed in Table S1 produce a m/z 16 fragment during mass spectrometry, which made the risk of misidentifying methane extremely high. Pure acetates evolved two m/z 18 peaks during EGA; the first peak between 100 °C and 250 °C was related to dehydration and the second consisted of H_2O and a m/z 18 fragment from acetic acid. Dispersing the acetates in fused silica altered the relative abundances of their organic pyrolysis products and caused many peaks to shift.

Perchlorates strengthened the CO_2, m/z 28_c, and H_2O evolutions from acetates and weakened or scrubbed their acetone and acetic acid releases. While the m/z 36 fragment from acetone was significant in the pure acetate data, in the perchlorate mixtures HCl was the dominant source of m/z 36. Chloromethane (m/z 50) was evolved by the majority of the acetate-perchlorate mixtures and hints of chloroacetone were observed when acetates were abundant relative to perchlorates. Chloromethane was distinguished from methyl-propene by examining how m/z 52 tracked with m/z 50. If m/z 50 and m/z 52 tracked each other at a ratio consistent with the ratio of $CH_3{}^{35}Cl$ to $CH_3{}^{37}Cl$, they were assigned to chloromethane (Figure S4).

3.3.1. Pyrolysis of Fe(II) Acetate

Pure Fe(II) acetate evolved an acetic acid peak at 290 °C and CO_2 and acetone peaks at 310 °C (Figure 4). The peaks were tracked by m/z 18, 28_c, 36, and 50, which were likely sourced predominantly from the organic products of acetate pyrolysis rather than H_2O, CO, HCl, and chloromethanes, as this was a pure

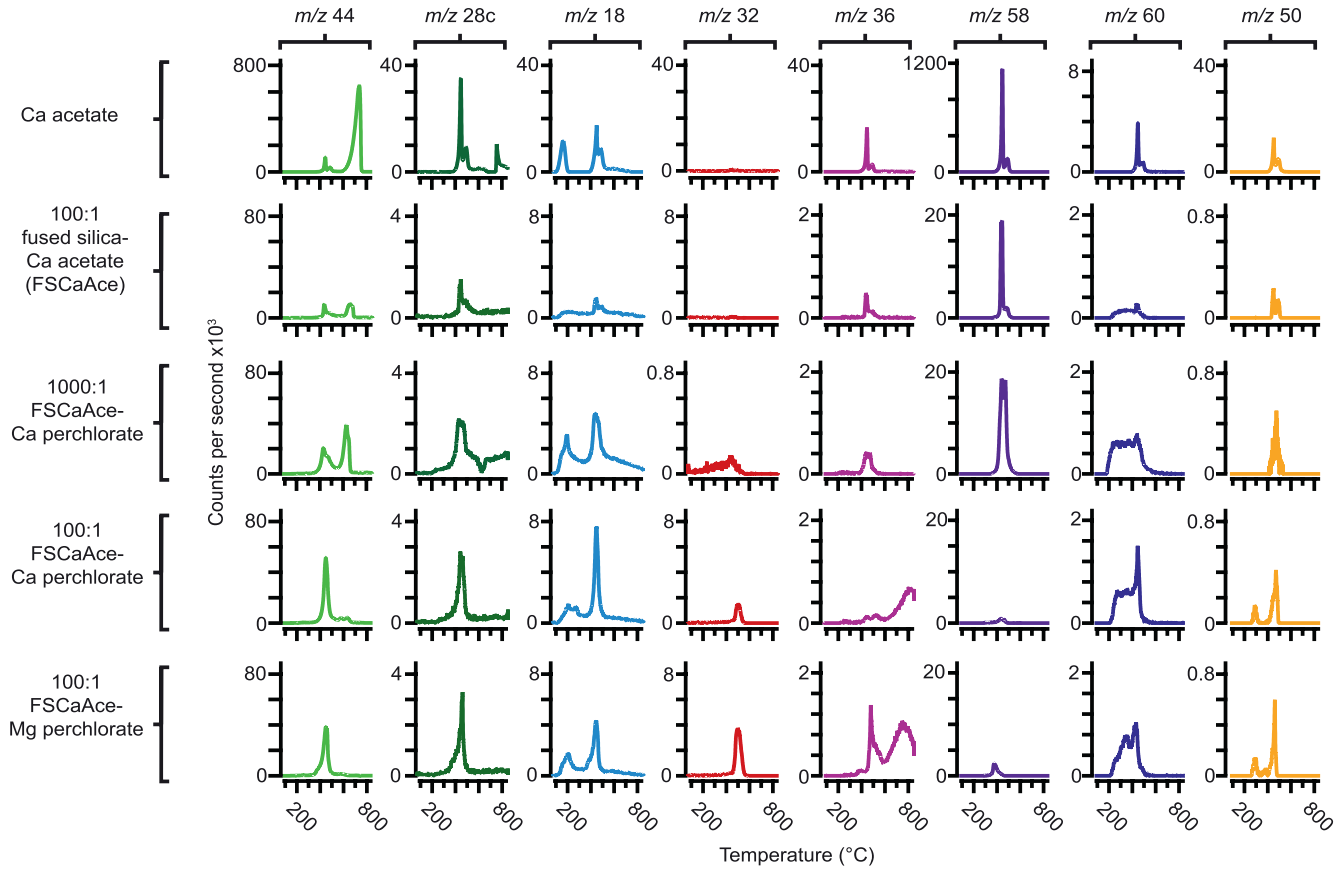

Figure 5. Evolved *m/z* 44 (CO_2, organic fragments), *m/z* 28_c (corrected CO, organic fragments), *m/z* 18 (H_2O, organic fragments), *m/z* 32 (O_2), *m/z* 36 (HCl, organic fragments), *m/z* 58 (acetone), *m/z* 60 (acetic acid), and *m/z* 50 (chloromethane, organic fragments) versus temperature as detected by SAM-like EGA of pure Ca acetate, FSCaAce, a 1000:1 FSCaAce and Ca perchlorate mixture, a 100:1 FSCaAce and Ca perchlorate mixture, and a 100:1 FSCaAce and Mg perchlorate mixture. It should be noted that a 1 mg aliquot was used for the pure acetate experiment, 7 mg aliquots for the 100:1 silica and silica-perchlorate mixtures, and a 20 mg aliquot for the 1000:1 mixture. EGA, evolved gas analysis; FSCaAce, a 100:1 mixture of fused silica and Ca acetate; SAM, Sample Analysis at Mars.

acetate run with no perchlorates present. A small 150 °C H_2O peak was observed as the acetate dehydrated. A high-temperature *m/z* 28_c peak was detected that was interpreted as instrumental in origin, as sporadic CO releases from the mass spectrometer filament are occasionally observed toward the end of lengthy EGA sequences.

When dispersed in fused silica at a 100:1 mixing ratio (FSFeIIAce), Fe(II) acetate produced broad CO_2, *m/z* 28_c, acetone, and acetic acid peaks at 330 °C. The 1000:1 FSFeIIAce-Ca-perchlorate mixture evolved two CO_2 peaks during EGA. The first peak at 300 °C occurred with a weak *m/z* 28_c release and a broad H_2O shoulder. The second peak at 365 °C was associated with a weak release of acetone. O_2 was not detected and no major HCl peak was observed.

When the 100:1 FSFeIIAce-perchlorate mixtures were pyrolyzed, the Fe(II) acetate CO_2 and *m/z* 28_c peaks shifted to 250-275 °C and acetone and acetic acid were no longer detected. Chloromethane was observed in the Mg-perchlorate mixture but not the Ca-perchlorate mixture, which was likely related to the earlier onset of Cl_2/HCl from Mg perchlorate relative to Ca perchlorate. Unlike the Fe oxalate experiments, where CO was completely scrubbed, weak CO peaks were detected. Fe(II) acetate is soluble in water but no evidence for cation exchange between the acetate and the perchlorate solutions was observed in the EGA data.

Each Fe(II)-acetate-perchlorate mixture produced a broad low-temperature H_2O release with shoulders that partly overlapped with CO_2, indicating oxidation, while the lower-temperature peaks were related

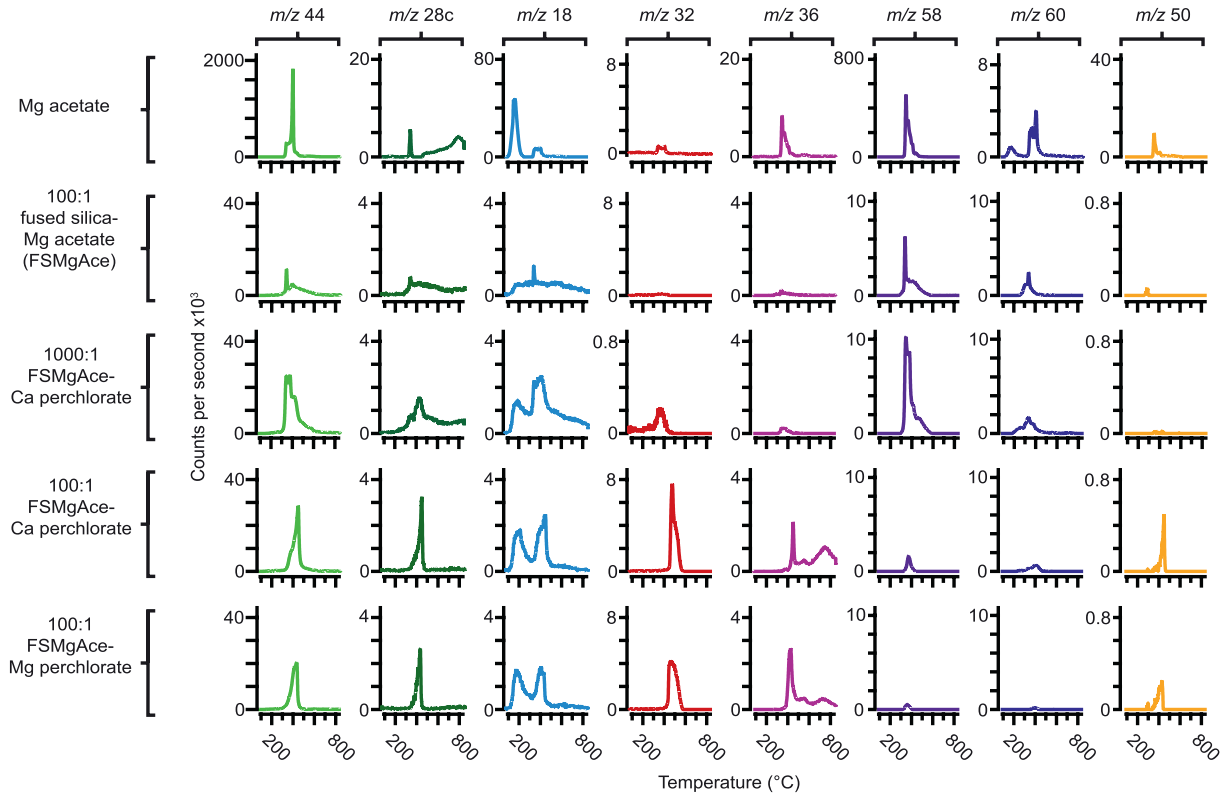

Figure 6. Evolved *m/z* 44 (CO_2, organic fragments), *m/z* 28_c (corrected CO, organic fragments), *m/z* 18 (H_2O, organic fragments), *m/z* 32 (O_2), *m/z* 36 (HCl, organic fragments), *m/z* 58 (acetone), *m/z* 60 (acetic acid), and *m/z* 50 (chloromethane, organic fragments) versus temperature as detected by SAM-like EGA of pure Mg acetate, FSMgAce, a 1000:1 FSMgAce and Ca perchlorate mixture, a 100:1 FSMgAce and Ca perchlorate mixture, and a 100:1 FSMgAce and Mg perchlorate mixture. It should be noted that a 1 mg aliquot was used for the pure acetate experiment, 7 mg aliquots for the 100:1 silica and silica-perchlorate mixtures, and a 20 mg aliquot for the 1000:1 mixture. EGA, evolved gas analysis; FSMgAce, a 100:1 mixture of fused silica and Mg acetate; SAM, Sample Analysis at Mars.

to dehydration of the silica, Fe(II) acetate, and perchlorates. The O_2 peaks from Ca and Mg perchlorate shifted to lower temperatures in the presence of Fe(II) acetate and chloromethane began to evolve from ~200 °C in both mixtures, indicating that chlorination reactions began at temperatures below the onset of HCl evolution in the perchlorate-only runs. The 100:1 FSFeIIAce-Ca-perchlorate mixture produced a strong high-temperature HCl peak and a weak HCl release coincident with the O_2 peak. The 100:1 FSFeIIAce-Mg-perchlorate mixture evolved a sharp HCl peak at low temperatures and a small peak at high temperatures, indicating that some $MgCl_2$ formed during the decomposition of Mg perchlorate.

3.3.2. Pyrolysis of Ca Acetate

Pure Ca acetate produced a very strong acetone peak, a *m/z* 44 peak, and an acetic acid peak at 445 °C during EGA, followed by smaller peaks for each species at 490 °C (Figure 5). Peaks for *m/z* 18, 28_c, 36, and 50 were also detected at 445 °C and 490 °C and the $CaCO_3$ formed by the thermal decomposition of Ca acetate evolved a major CO_2 peak at 735 °C. As with the Fe(II) acetate experiment, the Ca acetate run exhibited a high-temperature CO peak related to instrument background. When Ca acetate was dispersed in fused silica at a 100:1 ratio (FSCaAce), the CO_2 peak evolved by the $CaCO_3$ intermediate shifted 100 °C lower and weakened significantly but the 445 °C and 490 °C *m/z* 44 and acetone peaks were largely unaffected. This was similar to the behavior seen for the $CaCO_3$ intermediate formed by Ca oxalate when it was dispersed in silica. The acetic acid peak developed a broad low-temperature shoulder which began to evolve from 220 °C, suggesting hydrolysis related to the fused silica (Reaction 9 in Section 1).

Ca acetate continued to evolve prominent peaks for CO_2, acetone, and *m/z* 36 between 380 °C and 520 °C and a strong high-temperature CO_2 release from $CaCO_3$ in the 1000:1 FSCaAce-Ca-perchlorate mixture.

Peaks for *m/z* 18, 28_c, 50, and acetic acid were also detected, with the acetic acid release occurring between 180 °C and 550 °C, showing further evidence for acetate hydrolysis. A sharp H_2O release was detected at 200 °C. For the 100:1 FSCaAce-perchlorate mixtures, the initial CO_2 release from Ca acetate at ~445 °C strengthened but did not shift, while the high-temperature CO_2 peak from decomposition of the $CaCO_3$ intermediate was no longer detected. A minor CO_2 shoulder was observed, suggesting the carbonate rapidly decomposed in the presence of HCl. The low-temperature H_2O peaks sharpened and the higher-temperature H_2O releases due to oxidation strengthened significantly. The O_2 peaks from Ca and Mg perchlorate weakened but did not shift to lower temperatures in the presence of Ca acetate. Each Ca-acetate-perchlorate mixture evolved broad high-temperature HCl peaks above 600 °C and Mg perchlorate produced a strong mid-temperature HCl peak. The acetone releases from the 100:1 FSCaAce-perchlorate mixtures were significantly weakened, but in contrast to the Fe(II) acetate experiments they were not scrubbed. The acetic acid peaks strengthened slightly, and chloromethane releases were detected with the onset of the O_2 peaks.

3.3.3. Pyrolysis of Mg Acetate

Pure Mg acetate evolved H_2O and acetic acid peaks at 160 °C, acetone, acetic acid, *m/z* 18, 28_c, 36, 44, and *m/z* 50 peaks at 340 °C, and a strong CO_2 peak with minor acetic acid and *m/z* 18 at 400 °C (Figure 6). When Mg acetate was dispersed in fused silica at a 100:1 mixing ratio (FSMgAce), the 340 °C *m/z* 44 peak became more prominent and the 400 °C CO_2 peak broadened and extended to ~700 °C. The 400 °C CO_2 peak was likely related to the decomposition of a $MgCO_3$ intermediate as the peak began to evolve from 350 °C and had little associated *m/z* 28_c. The acetic acid peak observed at 160 °C for pure Mg acetate was no longer detected in silica, but a significant shoulder was observed prior to the major acetic acid peak at 340 °C. The acetone peak shape was relatively unchanged, but acetone and acetic acid were comparable in peak height, in contrast to the pure acetate where acetone was dominant.

EGA of the 1000:1 FSMgAce-Ca-perchlorate mixture produced CO_2 peaks at 340 °C and 380 °C and a significant high-temperature CO_2 shoulder. The CO_2 peaks were associated with releases of acetone, *m/z* 36, and acetic acid. The CO_2 shoulder was most prominent up to 430 °C but continued to 600 °C. A weak *m/z* 28_c release tracked CO_2. A broad H_2O peak occurred at 180 °C as the mixture dehydrated and a prominent H_2O release accompanied the CO_2 peaks.

The 100:1 FSMgAce-perchlorate mixtures produced CO_2 peaks between 400 °C and 450 °C, with each CO_2 profile featuring a minor shoulder that initiated at ~300 °C. The CO_2 releases were tracked by *m/z* 28_c. The Ca and Mg perchlorate O_2 peaks weakened but did not shift significantly in the presence of Mg acetate. Each Mg-acetate-perchlorate mixture evolved broad high-temperature HCl releases from ~600 °C and sharp HCl and chloromethane peaks were detected as O_2 began to evolve. Both the acetone and acetic acid releases from Mg acetate weakened substantially in the Ca- and Mg-perchlorate mixtures.

When FSCaAce and FSMgAce were mixed with Ca and Mg perchlorate, minor peaks such as *m/z* 92 ($^{35}ClCH_2COCH_3$) and *m/z* 94 ($^{37}ClCH_2COCH_3$) were observed that were suggestive of chloroacetone (Table S1; Figure S5). SAM-like pyrolysis-GC-MS of a 1000:1 FSMgAce-Ca-perchlorate mixture confirmed that chloroacetone was being produced. Chloroacetone was not identified in previous pyrolysis-GC-MS studies of a 100:1 FSMgAce-Ca-perchlorate mixture (M. Millan, personal communication, March 5, 2019), suggesting that elevated acetate concentrations relative to perchlorates would be required in a sample for chloroacetone to be observable by SAM.

3.3.4. Quantification of Acetate CO_2 Production During Pyrolysis

The H_2O profiles observed in Figures 4–6 were consistent with anhydrous Fe(II) oxalate, Ca acetate monohydrate, and Mg acetate tetrahydrate. The different acetate standards evolved highly variable amounts of CO_2 during EGA (Table 2; Table S6). It should be noted that the CO_2 production from pure acetates was quantified using the *m/z* 44_{CO2} traces. For the fused silica mixtures, *m/z* 44 and *m/z* 44_{CO2} matched well for major peaks but *m/z* 22 was too weak to assess minor *m/z* 44 evolutions so *m/z* 44 was used for quantification. Pure Fe(II), Ca, and Mg acetates evolved greater amounts of CO_2 than pure Fe(II), Ca, and Mg oxalates but after dispersal within FS-120 the oxalates produced stronger releases. The addition of minor Ca perchlorate to the acetate-fused-silica mixtures caused a moderate increase in the quantities of CO_2 evolved (that was within error of the perchlorate-free fused-silica mixtures). However, Fe(II) acetate appeared to evolve slightly less CO_2 (also within error). Higher concentrations of Ca perchlorate caused an increase in the CO_2

Table 2
The Quantities of CO_2 Produced by Acetates, Fused-Silica-Acetate Mixtures, and Fused-Silica-Acetate-Perchlorate Mixtures During EGA

Sample	Cation	CO_2 (μmol CO_2/mg anhydrous acetate salt)	Average CO_2 (μmol CO_2/mg anhydrous acetate salt)	1σ
Pure Acetates	Fe(II)	10.96 ± 0.10	17.15 ± 0.12	6.73
	Ca	16.19 ± 0.11		
	Mg	24.31 ± 0.14		
FSAce	Fe(II)	3.56 ± 1.64	7.31 ± 2.13	3.25
	Ca	9.20 ± 2.01		
	Mg	9.17 ± 2.75		
1000:1 FSAce-Ca perchlorate	Fe(II)	3.04 ± 0.58	7.90 ± 0.76	4.21
	Ca	10.32 ± 0.72		
	Mg	10.35 ± 0.98		
100:1 FSAce-Ca perchlorate	Fe(II)	4.10 ± 1.61	14.27 ± 2.12	8.97
	Ca	21.06 ± 2.02		
	Mg	17.65 ± 2.74		
100:1 FSAce-Mg perchlorate	Fe(II)	3.70 ± 1.58	11.40 ± 2.13	6.92
	Ca	17.10 ± 2.08		
	Mg	13.39 ± 2.75		
Average acetate CO_2 production at low O_2 concentrations			7.61 ± 1.45	3.38
Average acetate CO_2 production at high O_2 concentrations			12.83 ± 2.13	7.33

Abbreviations: EGA, evolved gas analysis; FSAce, 100:1 fused-silica-acetate mixtures.

quantities evolved by all of the acetates studied. Mg-perchlorate mixtures evolved slightly less CO_2 compared to the Ca-perchlorate mixtures, likely due to the lesser O_2 release from Mg perchlorate. Fe(II) acetate evolved significantly less CO_2 than Ca and Mg acetate. This is consistent with the thermal decomposition of Fe(II) acetate generating a greater proportion of the free metal compared to Ca and Mg acetate, which would have been an efficient sink for perchlorate O_2.

3.4. SAM CO_2 and CO Data

3.4.1. SAM CO_2 and CO EGA Data

The modern eolian materials analyzed by SAM (RN4, GB, and OG3 [Text S1]) produced similar EGA profiles for CO_2 and CO (Figure 7). Each eolian sample evolved two prominent CO_2 peaks between ~380 °C and 500 °C and low-temperature CO_2 shoulders, which began to evolve from ~100 °C to 150 °C. The CO_2 shoulder evolved by RN4 was substantially stronger than those seen in GB and OG3. Each run had extremely weak CO evolutions relative to CO_2, with minor peaks detected between ~280 °C and 340 °C.

The JK4 and CB3 samples from the Sheepbed mudstone produced sharp CO_2 peaks at ~260 °C–270 °C that were tracked by CO. The more intensely veined JK4 target also evolved a significant low-temperature CO_2 shoulder and a further CO_2 release at ~400 °C, which were not tracked by CO. The WJ sandstone target evolved CO_2 peaks at 180 °C and 420 °C. WJ CO was extremely weak relative to CO_2, with minor releases observed at 250 °C and 360 °C.

The first Murray formation targets, CH, MJ, TP, and BK all produced small CO_2 peaks at ~160 °C–170 °C, with no associated CO, and major CO_2 and CO releases at ~310 °C–330 °C. An additional CO_2 peak was observed at 590 °C in TP and a high-temperature CO release was detected in CH at ~750 °C. The Stimson sandstone parent rock sample BY evolved a major CO_2 peak at ~270 °C that was tracked by CO, while material from a nearby alteration halo (GH2) evolved a broad CO_2 peak at ~350 °C that was tracked by CO, and a sharp CO_2 peak at 500 °C, which had no associated CO. Both BY and GH2 produced CO_2 peaks at 160 °C.

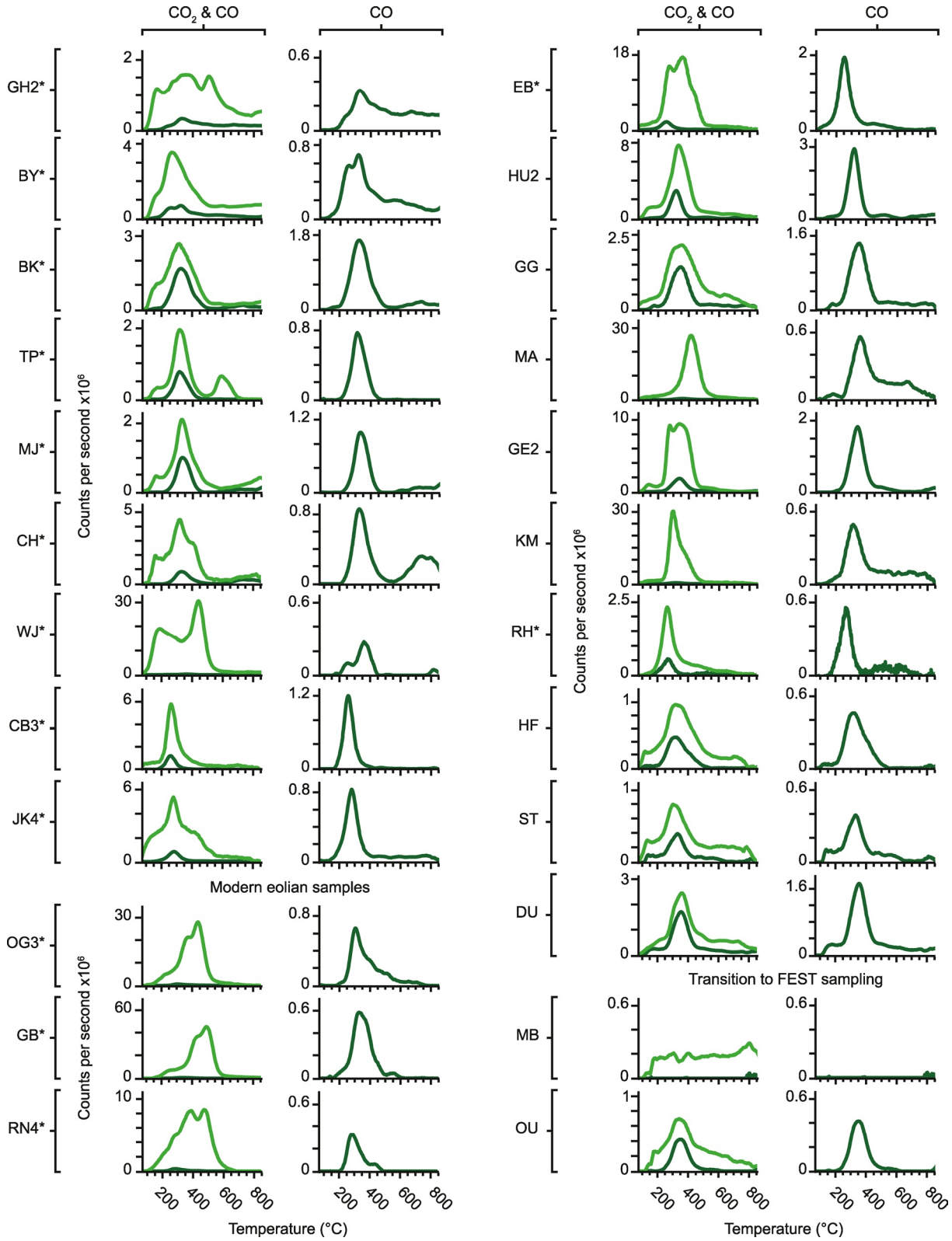

Figure 7. CO_2 and CO evolutions from Martian samples analyzed by SAM EGA. The modern eolian samples are plotted separately from samples acquired from ancient Gale crater rocks. SAM samples that evolved O_2 peaks are highlighted with an asterisk. Between acquisition of the MB and DU samples, MSL switched to the FEST method of drilling, due to a drill fault suspending standard drill operations. EGA, evolved gas analysis; MSL, Mars Science Laboratory; FEST, feed-extended sample transfer; SAM, Sample Analysis at Mars.

From the OU drill target onwards, the majority of SAM samples did not produce O_2 peaks during EGA, indicating that oxychlorines were either absent or at very low concentrations (Archer et al., 2018). OU produced a CO_2 peak at 180 °C and major CO_2 and CO peaks at ~340 °C–350 °C. MB produced no significant CO_2 or CO releases. In contrast to previous SAM runs, the DU sample evolved a low-temperature CO_2 release that was tracked by CO. DU also evolved strong CO_2 and CO peaks at 360 °C. The ST drill target from within the VRR evolved CO_2 and CO peaks at 140 °C and ~320 °C–330 °C. HF, from the gray Jura, evolved a CO_2 peak and minor CO at 120 °C and CO_2 and CO peaks at 320 °C. The red Jura sample, RH, evolved a prominent O_2 peak during EGA, indicating that oxychlorines were present. CO_2 and CO peaks were detected at 270 °C and no low-temperature CO_2 or CO releases were observed.

The first GT drill target, KM, evolved a sharp CO_2 peak at 300 °C and a very weak CO peak at 315 °C. The GE2 and MA samples from the Knockfarril Hill member evolved CO_2 and CO profiles that were distinctly different from both each other and KM. In GE2, CO_2 peaks were observed at 140 °C, 275 °C, and 340 °C and the 340 °C CO_2 release was accompanied by a weak CO peak. MA produced a strong CO_2 release at 415 °C and a very weak CO peak at 360 °C. In the fractured intermediate unit, the GG target evolved a broad CO_2 peak and a very strong CO release at 350 °C, while the HU2 sample produced CO_2 and CO peaks at ~335 °C. Both GG and HU2 produced low-temperature CO_2 releases, which in GG was associated with a minor CO peak. The EB sample from the pediment capping unit produced an O_2 peak during EGA and evolved major CO_2 peaks at 270 °C and 360 °C, a CO2 shoulder at 430 °C and a minor CO release at 255 °C.

SAM data were assessed for the presence of acetone and acetic acid by examining the traces for *m/z* 58 and *m/z* 60. The search for acetone was complicated by the ubiquitous presence of 2,2,2-trifluoro-N-methyl-acetamide (TFMA) in SAM runs, a by-product of the leaking wet chemistry cup. The major fragments produced by TFMA during mass spectrometry include *m/z* 58 and *m/z* 127. In every SAM run, *m/z* 58 peaks were observed <400 °C that tracked with *m/z* 127. Most SAM samples evolved *m/z* 58 and *m/z* 127 at a ratio consistent with TFMA (Eigenbrode et al., 2018). However, in RN4 *m/z* 58 features were observed at ~230 °C and ~360 °C that were slightly in excess of the expected ratio (Figure S6). Acetone was reported in SAM GC-MS studies of RN but was described as originating from the leaking wet chemistry reagents (Leshin et al., 2013) A similar *m/z* 58 feature was observed at 380 °C in WJ but was extremely weak. When *m/z* 60 releases were observed in SAM data they were typically small high-temperature peaks that tracked with masses suggestive of carbonyl sulfide rather than acetic acid. Peaks for *m/z* 92 and *m/z* 94 were occasionally observed in SAM data but never co-occurred at a ratio consistent with chloroacetone.

3.4.2. Quantitative SAM CO_2 and O_2 Data and Upper Limits for Organic Salts in Gale Crater

A comparison between quantitative SAM CO_2 data and our laboratory data enabled an estimation of the upper limits for oxalate and acetate concentrations in SAM samples (Table 3). The uncertainties for the estimates shown in Table 3 are large. This is due to the propagation of errors from the SAM instrument suite and our laboratory methods. The main findings of our comparison are that the majority of SAM samples have upper limits for organic salts well below 1 wt.%, but in a few select samples, organic salt concentrations may have been great enough to be observable by instruments other than SAM (discussed further in Section 4.4).

The modern eolian samples evolved substantial amounts of CO_2 and were calculated to have upper limits for organic salts between ~0.7 and 1.4 wt.%. During SAM's analyses of the Yellowknife Bay materials, JK4 evolved significantly more CO_2 than CB3 and had an upper limit for organic salts of ~0.7–0.8 wt.%. The Windjana target evolved greater amounts of CO_2 than both the Yellowknife Bay and Modern eolian samples, with calculated upper limits for organic salts of ~1.2–1.5 wt.%. From CH to RH, the Murray and Stimson samples typically evolved significantly less CO_2 and had upper limits <0.5 wt.%. The majority of GT samples and the EB sample from the Greenheugh Pediment capping unit evolved substantial amounts of CO_2 and had upper limits for organic salts of ~0.5–1.6 wt.%. The exceptions were GG, which had a very weak CO_2 release and an upper limit of only ~0.2–0.4 wt.% and KM, which evolved prodigious amounts of CO_2, but its CO_2 and CO peaks were not particularly good fits with our organic salt data.

Table 3
Upper Limits for Oxalates and Acetates in Gale Crater Samples

Mars sample	Evolved CO_2 (μmol/mg)[a]	Evolved O_2 (μmol/mg)[b]	Oxalate upper limit (wt.%)	Acetate upper limit (wt.%)
FEST-portioned drilled samples				
EB	0.123 ± 0.112	0.035 ± 0.026	0.75 ± 0.79	0.96 ± 1.03
HU2	0.059 ± 0.057	N.D.	0.53 ± 0.59	0.77 ± 0.89
GG	0.027 ± 0.042	N.D.	0.24 ± 0.42	0.35 ± 0.63
MA	0.125 ± 0.074	N.D.	1.13 ± 0.83	1.64 ± 1.29
GE2	0.105 ± 0.076	N.D.	0.95 ± 0.82	1.39 ± 1.26
KM	0.271 ± 0.142	N.D.	2.45 ± 1.62	3.56 ± 2.55
RH	0.033 ± 0.068	0.104 ± 0.092	0.20 ± 0.45	0.26 ± 0.57
HF	0.024 ± 0.064	N.D.	0.21 ± 0.60	0.31 ± 0.90
ST	0.025 ± 0.058	N.D.	0.23 ± 0.56	0.33 ± 0.83
DU	0.015 ± 0.014	N.D.	0.14 ± 0.14	0.20 ± 0.22
CHIMRA-portioned drilled samples				
MB	0.007 ± 0.029	N.D.	0.06 ± 0.28	0.09 ± 0.40
OU	0.004 ± 0.020	N.D.	0.04 ± 0.19	0.06 ± 0.27
GH2	0.020 ± 0.011	0.024 ± 0.008	0.12 ± 0.09	0.16 ± 0.11
BY	0.040 ± 0.031	0.027 ± 0.011	0.24 ± 0.23	0.31 ± 0.30
BK	0.022 ± 0.021	0.067 ± 0.024	0.14 ± 0.14	0.17 ± 0.19
TP	0.013 ± 0.025	0.018 ± 0.009	0.08 ± 0.17	0.10 ± 0.21
MJ	0.036 ± 0.061	0.080 ± 0.043	0.22 ± 0.40	0.28 ± 0.52
CH	0.076 ± 0.064	0.013 ± 0.008	0.46 ± 0.45	0.59 ± 0.59
WJ	0.198 ± 0.097	0.047 ± 0.015	1.21 ± 0.76	1.54 ± 1.01
CB3	0.049 ± 0.033	0.220 ± 0.115	0.30 ± 0.24	0.38 ± 0.32
JK4	0.107 ± 0.072	0.020 ± 0.010	0.65 ± 0.53	0.83 ± 0.70
Modern eolian materials				
OG3	0.107 ± 0.051	0.033 ± 0.012	0.65 ± 0.40	0.83 ± 0.54
GB	0.169 ± 0.090	0.047 ± 0.017	1.03 ± 0.69	1.32 ± 0.92
RN average	0.180 ± 0.067	0.078 ± 0.042	1.10 ± 0.56	1.40 ± 0.75

Abbreviations: BK, Buckskin; BY, Big Sky; CH, Confidence Hills; CHIMRA, Collection and Handling for Interior Martian Rock Analysis; DU, Duluth; EB, Edinburgh; FEST, feed-extended sample transfer; GB, Gobabeb; GG, Glasgow; HF, Highfield; KM, Kilmarie; MA, Mary Anning; MB, Marimba; MJ, Mojave; OU, Oudam; RH, Rock Hall; RN, Rocknest; ST, Stoer; TP, Telegraph Peak; WJ, Windjana.
[a]CO_2 corrected for contributions from leaking wet chemistry reagents. [b]N.D. indicates no detection.

4. Discussion and Implications

4.1. General Discussion

Our laboratory investigations have demonstrated how dispersal within a matrix and mixing with perchlorates can have a substantial impact on the thermal decomposition of oxalates and acetates. A number of the pure organic salts we examined formed carbonate intermediates during pyrolysis, with Ca oxalate and Ca acetate forming a secondary CO_2 peak as their $CaCO_3$ intermediates decomposed at higher temperatures. Dispersal within fused silica appeared to impede carbonate formation from organic salts, resulting in a stronger initial CO_2 release from the oxalate or acetate and a weaker secondary CO_2 peak in the case of Ca oxalate and Ca acetate. Additionally, while acetone was a dominant product of the decomposition of pure Mg acetate, in fused silica the acetone and acetic acid peaks were comparable in size. Dehydration of the fused silica and perchlorates also led to broader acetic acid peaks due to acetate hydrolysis.

The oxalates we studied in this work can be split into two groups based on how they responded to the presence of perchlorates during pyrolysis. Fe oxalates, which readily undergo oxidation of their solid pyrolysis products, evolved broad low-temperature CO_2 releases and the sharp CO peaks that were observed in the pure Fe oxalate runs were scrubbed. Ca and Mg oxalates, whose solid pyrolysis products do not undergo further oxidation, experienced minimal shifting of their CO_2 and CO peaks, though the CO releases did weaken. The carbonate intermediates formed by Ca and Mg oxalates were inferred to have reacted with the HCl/Cl_2 produced by perchlorates, which resulted in enhanced CO_2 production and further weakening of the secondary CO_2 peak from $CaCO_3$. When minor amounts of Ca perchlorate were mixed with Fe oxalates, high-temperature HCl peaks were observed but the O_2 from the perchlorate was completely consumed by oxidation reactions. In contrast, the Ca- and Mg-oxalate mixtures with minor Ca perchlorate concentrations produced sharp O_2 peaks but small or absent HCl peaks.

Perchlorates enhanced the CO_2, H_2O, and CO releases from acetates due to oxidation and combustion. They also shifted the Mg acetate CO_2 peak to slightly higher temperatures and the Fe(II) acetate CO_2 peak to lower temperatures. The CO_2 release from the $CaCO_3$ intermediate formed by Ca acetate decomposition appeared to be scrubbed more readily than that formed by Ca oxalate, as no secondary CO_2 peak was observed at elevated perchlorate concentrations. All of the acetates studied showed significant weakening of their acetone peaks in the presence of perchlorates and Fe(II) acetate seemed to be particularly susceptible to having both its acetone and acetic acid releases scrubbed.

The majority of our acetate-perchlorate runs evolved chloromethane, which in SAM data is generally interpreted as a by-product of the leaking wet chemistry reagents (Freissinet et al., 2015; Glavin et al., 2013; Leshin et al., 2013; Szopa et al., 2020). Our results suggest that Martian acetates, if present, could contribute to low-temperature SAM chloromethane detections, such as those seen in RN (Leshin et al., 2013). We also observed chloroacetone in our data, but only when acetates were abundant relevant to perchlorates, which suggests the formation of significant amounts of chloroacetone from acetates in a flight instrument on Mars would be unlikely. SAM wet chemistry data should be assessed for possible derivatization or thermochemolysis products of organic salts, but such a study is outside the scope of this paper.

The O_2 peaks evolved by Ca and Mg perchlorate generally shifted to lower temperatures when mixed with Fe oxalates and Fe acetates. In addition, the generation of chloromethane from the Fe(II)-acetate-perchlorate mixtures occurred at temperatures below the onset of HCl in the perchlorate-only experiments. These observations suggest that the presence of Fe-bearing organic salts lowered the decomposition temperature of Ca and Mg perchlorates, which resulted in O_2 releases that were a better fit with many SAM O_2 peaks (Sutter et al., 2017).

4.2. Implications for SAM CO_2 and CO Data

Organic salts have previously been described as potential contributors to SAM CO_2 and CO peaks (Applin et al., 2015; Eigenbrode et al., 2014; Franz et al., 2020; McAdam, Sutter, Archer, Franz, Wong, et al., 2020; Ming et al., 2014; Stern et al., 2018; Sutter et al., 2017). Applin et al. (2015) stated that the major CO_2 releases in RN EGA data were consistent with the decomposition of Fe and Mg oxalates mixed with Fe and Mg carbonates. Our data agree that Mg oxalate could have been responsible for the 470 °C CO_2 peak in RN4, but Fe oxalates would have been unlikely contributors to the CO_2 release at 380 °C because of the presence of oxychlorines, inferred from the observation of a strong evolved O_2 peak. If Fe oxalates and Fe acetates were present in RN4 it was more likely they would have contributed to the substantial CO_2 shoulder <300 °C (Figure S7). The CO_2 peaks generated by our mixtures of Ca or Mg acetate with perchlorates were a closer fit with the 380 °C peak in RN4. The CO_2 peaks observed between ~400 °C and 500 °C in GB and OG3 were consistent with the decomposition of a mixture of Ca acetate, Mg acetate, Mg oxalate, and perchlorates.

If organic salts were present in the modern eolian materials analyzed by SAM, our laboratory results demonstrate that the lack of acetone, acetic acid, and major CO peaks in SAM EGA data could be due to perchlorates. CO may also have reacted with other gases in the SAM oven or undergone disproportionation (Newsome, 1980; Vedyagin et al., 2016). If Mg oxalates and Ca or Mg acetates were significant CO_2 contributors in GB and OG3 it would suggest that a unit with appreciably high levels of these phases exists somewhere within Gale crater. If such a unit can form at one locality on Mars, it is likely that organic salt

deposits could occur elsewhere on the planet. Possible spectral signatures of Mg oxalates have been detected in an unnamed ~61 km crater located at 37.07°S, 178.23°W using Compact Reconnaissance Imaging Spectrometer for Mars (CRISM) data (Aaron et al., 2019). If the substantial low-temperature CO_2 evolutions seen in RN were due to Fe oxalates and Fe acetates, it would suggest they were present in the dust-sized fraction and that they could be a constituent of regional or global dust.

The drill samples acquired by MSL between the JK and GH sampling sites evolved O_2 peaks during SAM EGA and were therefore compared to the laboratory EGA data from our organic salt mixtures with elevated perchlorate concentrations. The major CO_2 and CO peaks produced by JK4 and CB3 at ~260 °C–270 °C were similar to our Fe(II) acetate data, while the additional CO_2 releases in JK4 were more consistent with Fe oxalates. If organic salts were significant contributors to the JK4 and CB3 CO_2 and CO peaks, it appears the more extensive veining experienced by JK4 may have led to a greater diversity of organic salt species in JK relative to CB. The WJ sandstone sample produced a low-temperature CO_2 peak that was comparable with our Fe-oxalate data and a 420 °C CO_2 peak that was similar to our Mg acetate CO_2 evolutions but the 420 °C peak did not track with CO. The first Murray formation targets (CH, MJ, TP, and BK) evolved low-temperature CO_2 peaks with no associated CO that were consistent with our Fe-oxalate mixtures, but the higher temperature CO_2 and CO evolutions from CH, MJ, TP, and BK did not fit well with our data (our Fe(II) acetate profiles were the closest fit). The BY parent rock and GH2 alteration halo materials from the Stimson sandstone also evolved low-temperature CO_2 peaks that were consistent with Fe-oxalates. The major ~270 °C CO_2 peak produced by BY was similar to our Fe(II)-acetate data, while the mid-temperature peak in GH2 was significantly broader. GH2 also featured a 500 °C CO_2 peak that fit well with our Mg-oxalate results. The more complex CO_2 profile of GH2 relative to BY was similar to the contrast between JK4 and CB3, which further suggests that some low-temperature alteration in Gale crater may have been associated with organic salt formation.

From OU onwards, the majority of SAM samples lacked O_2 peaks and were compared to our mixtures with minor or absent perchlorates. The major CO_2 peak evolved by OU fit well with our Fe(II) acetate data but the strong CO release in OU, and the lack of acetone or acetic acid, challenged an acetate explanation. Samples acquired on or around the VRR (DU, ST, HF, and the O_2-evolving RH) produced CO_2 peaks that fit extremely well with our Fe(II) acetate CO_2 data, which included perfectly matching the shift of the Fe(II) acetate CO_2 peak to lower temperatures in presence of O_2. However, as with OU, no acetone or acetic acid peaks were observed in VRR data. The low-temperature CO_2 releases seen in DU, ST, and HF were accompanied by CO peaks, which contrasted with the low-temperature CO_2 releases produced by many O_2-evolving SAM samples that had no associated CO. This behavior was similar to our laboratory observations for Fe oxalates but the CO_2 and CO peaks in DU, ST, and HF occurred at significantly lower temperatures than would be expected for an Fe oxalate in the absence of perchlorates.

The first GT sample, KM, evolved a major CO_2 peak at a similar temperature to our Fe(II) acetate experiments, but the KM CO peak was very weak and offset from the CO_2 release. The other GT samples (GE2, MA, GG, and HU2) produced CO_2 profiles that were more consistent with Fe(II) oxalate. However, the MA CO peak was offset from CO_2 and the GE2, MA, and HU2 major CO_2 and CO peaks occurred ~50 °C–100 °C lower than our laboratory data. If Fe(II) oxalates were present in GT, they appear to have persisted in forms somewhat different from the pure crystalline phases we examined. The numerous fits between SAM data and our Fe(II)-bearing organic salt data are not necessarily incompatible with sediments that were deposited under oxidizing conditions as Fe(III) oxalate has been shown to decompose to Fe(II) oxalate under gamma radiation (Saito et al., 1965). The O_2-evolving EB sample from the pediment capping unit produced a complex CO_2 profile that was consistent with a mixture of Fe oxalate, Fe acetate, Ca acetate, and Mg acetate with perchlorates.

While perchlorates and acetates are generally highly soluble in water, oxalates often have very low solubilities, including Ca, Mg, and Fe oxalates (Cheng et al., 2016). These differences in solubility challenge the hypothesis that perchlorates, acetates, and oxalates could be present in the same Martian unit. However, oxalates can become appreciably soluble in acidic solutions and are known to react with sulfuric acid to form sulfates and oxalic acid (Cromack et al., 1979; Sasaki, 1971). As the Martian atmosphere thinned in the late-Noachian and Hesperian, the SO_2 content of volcanic gases increased, leading to widespread acidic fluids that may have interacted with ancient organic salt deposits (Gaillard et al., 2013). Given that

alteration of organic matter by radiation and volcanism can also lead to organic salt formation, it is possible that oxalates and acetates of a variety of ages and origins could be present within Martian units of interest (Benner et al., 2000; Hofmann & Bernasconi, 1998).

4.3. Implications for Past Missions

Two previous successful missions to Mars have combined thermal extraction with mass spectrometry, the Viking Landers and the Phoenix Lander (Biemann et al., 1976; Hoffman et al., 2008). While the pyrolysis methods used by these missions differed significantly from those of SAM, high level interpretations about their results can still be discussed based on our laboratory data. The Viking ovens pyrolyzed Martian materials at 50 °C, 200 °C, 350 °C, and 500 °C (Biemann et al., 1976). The targets examined by Viking Lander 2 evolved CO_2 at each heating step but CO_2 quantification for the Viking Lander 1 experiments was not possible due to the use of CO_2 as a purge gas (Biemann et al., 1976, 1977). Our data show that Fe, Ca, and Mg oxalates and acetates would likely all evolve CO_2 in the temperature range used by the Viking ovens. The lack of indigenous acetone and acetic acid in Viking data was used by Benner et al. (2000) to rule out the presence of acetates in Viking samples. However, if sufficient concentrations of perchlorates were present, the acetone and acetic acid evolved by Martian acetates may have been scrubbed. The detection limits for acetone were also extremely high for some of the Viking experiments (Biemann et al., 1976). Chloromethanes were present in Viking data and our results show that interactions between perchlorates and acetates during heating can form such species (Biemann et al., 1976, 1977). No evidence for chloroacetone was found in our reanalysis of Viking GC-MS data.

Interpretations about Phoenix's Thermal and Evolved Gas Analyzer (TEGA) CO_2 data were assisted by supporting information from the lander's Wet Chemistry Laboratory (WCL), which revealed the presence of perchlorates and soils that were capable of buffering against acid addition (Boynton et al., 2009; Sutter et al., 2012). TEGA detected a CO_2 release between 725 °C and 820 °C, which was consistent with the decomposition of calcite, ankerite, or dolomite (Sutter et al., 2012). A CO_2 release between 400 °C and 680 °C was attributed to Mg carbonate, Fe carbonate, adsorbed CO_2, or organic molecules converted to CO_2 by soil oxidants (Sutter et al., 2012). Our data show that Mg or Ca oxalates could potentially contribute to the 400 °C–680 °C CO_2 release. If Ca oxalate was present, its $CaCO_3$ intermediate may also have contributed to the 725 °C–820 °C CO_2 peak. Ca and Mg acetate could also evolve CO_2 in the 400 °C–680 °C range, with the acetone and acetic acid scrubbed by perchlorates.

4.4. Implications for X-Ray Diffraction on Mars

In addition to SAM, MSL's analytical capabilities include X-ray diffraction (XRD) via the Chemistry and Mineralogy (CheMin) instrument (Blake et al., 2012). CheMin XRD analyses enable the identification and quantification of minerals present above ~1–2 wt%. Like inorganic minerals, XRD can characterize organic salts in the geological record (e.g., Echigo & Kimata, 2010), and we expect the same capabilities from CheMin if organic salts are present above the instrument detection limit. For Ca oxalates (mono, di, and tri-hydrate), the most intense diffraction peaks occur between ~6.2 and 5.0 Å (~16.6°–18.8°2θ, Co-Kα), a region of the pattern with few peaks from common, Martian rock-forming minerals. For Fe(II) oxalate (anhydrous), the most intense peak occurs at ~5.2 Å, and the most intense peak of Mg oxalate (dihydrate) occurs at ~4.9 Å. As illustrated by Applin et al. (2015), Fe(II) oxalate peaks are close to olivine and/or plagioclase peaks, a complicating factor to identifying this phase. Most samples analyzed by MSL, however, are olivine-poor or lack olivine, increasing the probability for Fe(II) oxalate detection using the peak at ~5.2 Å. An additional complicating factor is that Fe(II) and Mg oxalate overlap with some Fe sulfates and many Mg sulfates. To date, jarosite is the only crystalline Fe sulfate identified in CheMin XRD data, but future analyses of Mg sulfate-rich rocks may inhibit oxalate detection by XRD.

Our upper limits for oxalate and acetate concentrations in SAM samples (Table 3) highlighted several samples where, if a crystalline oxalate or acetate was the dominant contributor to SAM CO_2, its abundances would be near or above the CheMin detection limit. If a future SAM sample evolves extremely large amounts of CO_2, the corresponding CheMin data should be thoroughly assessed for the presence of crystalline organic salts.

4.5. Implications for Future Flight Experiments

The science payloads of upcoming missions to Mars will feature instruments capable of laser-desorption-ionization-mass-spectrometry (LDI-MS) and Raman spectroscopy (Goesmann et al., 2017; Rull et al., 2017; Wiens et al., 2021; Williford et al., 2018). Given that SAM data are potentially consistent with organic salts being widespread on Mars, it is of great importance that flight-like LDI-MS and Raman studies of oxalates and acetates are carried out in the laboratory. In addition to examining whether such methods can conclusively identify organic salts in complex Mars analogs, it would be imperative to establish if organic salts can complicate their search for other forms of organic matter and potential biosignatures.

5. Conclusions

Our laboratory pyrolysis studies of organic salts as pure phases, as trace phases mixed with silica, and in mixtures with perchlorate salts produced CO_2 peaks that were similar to many of the CO_2 releases detected by the SAM instrument suite on Mars. In our experiments, dispersal within a silica matrix was observed to alter the relative abundances of organic salt pyrolysis products and perchlorates were found to dramatically enhance the CO_2 evolutions from oxalates and acetates. We also discovered that mixing Ca or Mg perchlorate with Fe-bearing organic salts shifted the perchlorate O_2 peaks to lower temperatures, which resulted in better fits with many SAM O_2 releases. In addition, our acetate-perchlorate mixtures evolved chloromethane, which is commonly observed in Mars pyrolysis data. When acetate concentrations were elevated relative to perchlorates, chloroacetone was detected but no signals for chloroacetone were found during our assessment of SAM and Viking data.

The best fits between our laboratory data and SAM data occurred for oxychlorine-bearing Martian materials from modern eolian deposits and sedimentary rocks with evidence for low-temperature alteration. The modern eolian materials evolved CO_2 profiles that were consistent with the decomposition of mixtures of Fe, Ca, and Mg oxalates and acetates in the presence of perchlorates. At localities where Martian samples were drilled from both parent rock and altered rock, the altered targets tended to evolve more complex CO_2 profiles, potentially suggestive of an increase in organic salt diversity relative to the parent rock.

It was more challenging to find compelling fits between our laboratory data and SAM data for Martian materials that did not evolve O_2 peaks. For example, the VRR samples produced CO_2 peaks that were an excellent match with our Fe(II) acetate CO_2 profiles but the absence of acetone and acetic acid in SAM data challenged an acetate explanation. Many oxychlorine-free SAM samples produced CO_2 and CO profiles that were similar to those produced by our Fe oxalate standards but often at significantly lower temperatures. If Fe oxalates were present in these targets, they likely persisted in forms that were different from the pure crystalline phases we examined in the laboratory.

Our quantitative data comparisons identified several SAM samples, such as the modern eolian materials, where the upper limits for organic salt abundances were elevated and on the order of ~1–2 wt.%. If crystalline organic salts were present at these concentrations in a Martian sample, techniques such as XRD could potentially be able to make the first conclusive in situ detection of such a phase on Mars. The numerous fits between our laboratory data and SAM data emphasize the need for future orbital and surface investigations dedicated to investigating the nature and distribution of organic salts on Mars.

Acknowledgments
J. M. T. Lewis received support from the Center for Research and Exploration in Space Science and Technology (CRESST) II Cooperative Agreement (80GSFC17M0002). J. M. T. Lewis and C. N. Achilles acknowledge funding from the NASA Postdoctoral Program (NNH15CO48B), managed by Universities Space Research Association (USRA). J. L. Eigenbrode and A. C. McAdam were supported by the NASA ROSES MSL Participating Scientist Program. The authors are grateful for the knowledge and guidance of the wider MSL and SAM science and engineering teams. The authors thank S. T. Wieman for assistance in acquiring the Bamford and Tipper (1980) and Galwey and Brown (1999) reference books. The authors also thank two anonymous reviewers for their helpful comments.

Data Availability Statement

The laboratory data used in this project are available via Harvard Dataverse (Lewis, 2021). SAM data can be accessed via the Planetary Data System http://pds-geosciences.wustl.edu/missions/msl/.

References

Aaron, L. M., Steele, A., Shkolyar, S., Seelos, K., Viviano, C., Applin, D., et al. (2019). Detecting oxalate minerals on Mars using CRISM and in-situ spectroscopy. *Paper presented at the 50th Lunar and Planetary Science Conference, The Woodlands, TX*.

Afzal, M., Butt, P. K., & Ahmad, H. (1991). Kinetics of thermal decomposition of metal acetates. *Journal of Thermal Analysis*, *37*(5), 1015–1023. https://doi.org/10.1007/bf01932799

Applin, D. M., Izawa, M. R. M., Cloutis, E. A., Goltz, D., & Johnson, J. R. (2015). Oxalate minerals on Mars? *Earth and Planetary Science Letters*, *420*, 127–139. https://doi.org/10.1016/j.epsl.2015.03.034

Archer, P. D., Jr., Franz, H. B., Sutter, B., Arevalo, R. D., Jr., Coll, P., Eigenbrode, J. L., et al. (2014). Abundances and implications of volatile-bearing species from evolved gas analysis of the Rocknest aeolian deposit, Gale Crater, Mars. *Journal of Geophysical Research: Planets*, *119*(1), 237–254. https://doi.org/10.1002/2013je004493

Archer, P. D., Jr., Ming, D. W., Sutter, B., Hogancamp, J. V., Morris, R. V., Clark, B. C., et al. (2018). Oxychlorine detection in Gale crater, Mars and implications for past environmental conditions. *Paper presented at the Fall AGU Meeting, Washington, DC*.

Bamford, C. H., & Tipper, C. F. H. (1980). Chemical kinetics. In Reactions in the solid state (Vol. 22). Amsterdam: Elsevier.

Bell, J. L. S., Palmer, D. A., Barnes, H. L., & Drummond, S. E. (1994). Thermal decomposition of acetate: III. Catalysis by mineral surfaces. *Geochimica et Cosmochimica Acta*, *58*(19), 4155–4177. https://doi.org/10.1016/0016-7037(94)90271-2

Benner, S. A., Devine, K. G., Matveeva, L. N., & Powell, D. H. (2000). The missing organic molecules on Mars. *Proceedings of the National Academy of Sciences of the United States of America*, *97*(6), 2425–2430. https://doi.org/10.1073/pnas.040539497

Biemann, K., & Lavoie, J. M. (1979). Some final conclusions and supporting experiments related to the search for organic compounds on the surface of Mars. *Journal of Geophysical Research*, *84*(B14), 8385–8390. https://doi.org/10.1029/jb084ib14p08385

Biemann, K., Oro, J., Toulmin, P., III, Orgel, L. E., Nier, A. O., Anderson, D. M., et al. (1976). Search for organic and volatile inorganic compounds in two surface samples from the Chryse Planitia region of Mars. *Science*, *194*(4260), 72–76. https://doi.org/10.1126/science.194.4260.72

Biemann, K., Oro, J., Toulmin, P., III, Orgel, L. E., Nier, A. O., Anderson, D. M., et al. (1977). The search for organic substances and inorganic volatile compounds in the surface of Mars. *Journal of Geophysical Research*, *82*(28), 4641–4658. https://doi.org/10.1029/js082i028p04641

Blake, D. F., Morris, R. V., Kocurek, G., Morrison, S. M., Downs, R. T., Bish, D., et al. (2013). Curiosity at Gale Crater, Mars: Characterization and analysis of the Rocknest sand shadow. *Science*, *341*(6153), 1239505. https://doi.org/10.1126/science.1239505

Blake, D. F., Vaniman, D., Achilles, C., Anderson, R., Bish, D., Bristow, T., et al. (2012). Characterization and calibration of the CheMin mineralogical instrument on Mars Science Laboratory. *Space Science Reviews*, *170*(1–4), 341–399. https://doi.org/10.1007/s11214-012-9905-1

Boynton, W. V., Ming, D. W., Kounaves, S. P., Young, S. M. M., Arvidson, R. E., Hecht, M. H., et al. (2009). Evidence for calcium carbonate at the Mars Phoenix landing site. *Science*, *325*(5936), 61–64. https://doi.org/10.1126/science.1172768

Bristow, T. F., Rampe, E. B., Achilles, C. N., Blake, D. F., Chipera, S. J., Craig, P., et al. (2018). Clay mineral diversity and abundance in sedimentary rocks of Gale crater, Mars. *Science advances*, *4*(6). https://doi.org/10.1126/sciadv.aar3330

Broadbent, D., Dollimore, D., & Dollimore, J. (1967). The thermal decomposition of oxalates. Part IX. The thermal decomposition of the oxalate complexes of iron. *Journal of the Chemical Society A*, 451–454. https://doi.org/10.1039/j19670000451

Bryk, A. B., Dietrich, W. E., Lamb, M. P., Grotzinger, J. P., Vasavada, A. R., Stack, K., et al. (2020). New evidence for climate and erosion history in Gale crater, Mars, from Curiosity's ascent onto the Greenheugh pediment. *Paper presented at the Fall AGU Meeting, San Francisco, CA*.

Cannon, K. M., Sutter, B., Ming, D. W., Boynton, W. V., & Quinn, R. (2012). Perchlorate induced low temperature carbonate decomposition in the Mars Phoenix Thermal and Evolved Gas Analyzer (TEGA). *Geophysical Research Letters*, *39*(13). https://doi.org/10.1029/2012gl051952

Cheng, Z. Y., Fernández-Remolar, D. C., Izawa, M. R. M., Applin, D. M., Chong Díaz, M., Fernandez-Sampedro, M. T., et al. (2016). Oxalate formation under the hyperarid conditions of the Atacama Desert as a mineral marker to provide clues to the source of organic carbon on Mars. *Journal of Geophysical Research: Biogeosciences*, *121*(6), 1593–1604. https://doi.org/10.1002/2016jg003439

Chun, S. F. S., Pang, K. D., Cutts, J. A., & Ajello, J. M. (1978). Photocatalytic oxidation of organic compounds on Mars. *Nature*, *274*(5674), 875–876. https://doi.org/10.1038/274875a0

Clark, J. V., Sutter, B., McAdam, A. C., Rampe, E. B., Archer, P. D., Ming, D. W., et al. (2020). High-temperature HCl evolutions from mixtures of perchlorates and chlorides with water-bearing phases: Implications for the SAM instrument in Gale Crater, Mars. *Journal of Geophysical Research: Planets*, *125*(2), e2019JE006173. https://doi.org/10.1029/2019je006173

Conrad, P. G., Eigenbrode, J. L., Von der Heydt, M. O., Mogensen, C. T., Canham, J., Harpold, D. N., et al. (2012). The Mars science laboratory organic check material. *Space Science Reviews*, *170*(1–4), 479–501. https://doi.org/10.1007/s11214-012-9893-1

Cromack, K., Jr., Sollins, P., Graustein, W. C., Speidel, K., Todd, A. W., Spycher, G., et al. (1979). Calcium oxalate accumulation and soil weathering in mats of the hypogeous fungus Hysterangium crassum. *Soil Biology and Biochemistry*, *11*(5), 463–468. https://doi.org/10.1016/0038-0717(79)90003-8

Dartnell, L. R. (2011). Ionizing radiation and life. *Astrobiology*, *11*(6), 551–582. https://doi.org/10.1089/ast.2010.0528

Dartnell, L. R., Desorgher, L., Ward, J. M., & Coates, A. J. (2007). Modelling the surface and subsurface martian radiation environment: Implications for astrobiology. *Geophysical Research Letters*, *34*(2). https://doi.org/10.1029/2006gl027494

Dartnell, L. R., Page, K., Jorge-Villar, S. E., Wright, G., Munshi, T., Scowen, I. J., et al. (2012). Destruction of Raman biosignatures by ionising radiation and the implications for life detection on Mars. *Analytical and Bioanalytical Chemistry*, *403*(1), 131–144. https://doi.org/10.1007/s00216-012-5829-6

de Souza, A. O., Biondo, V., Ivashita, F. F., Nunes, G. C. D. S., & Paesano, A., Jr. (2017). Structural and magnetic characterization of nanostructured iron acetate. *Orbital: The Electronic Journal of Chemistry*, *9*(4), 261–265. https://doi.org/10.17807/orbital.v9i4.1006

Dollimore, D., & Griffiths, D. L. (1970). Differential thermal analysis study of various oxalates in oxygen and nitrogen. *Journal of Thermal Analysis*, *2*(3), 229–250. https://doi.org/10.1007/bf01911405

Echigo, T., & Kimata, M. (2010). Crystal chemistry and genesis of organic minerals: A review of oxalate and polycyclic aromatic hydrocarbon minerals. *The Canadian Mineralogist*, *48*(6), 1329–1357. https://doi.org/10.3749/canmin.48.5.1329

Eigenbrode, J. L., Bower, H., & Archer, P., Jr. (2014). Decarboxylation of carbon compounds as a potential source for CO2 and CO observed by SAM at Yellowknife Bay, Gale Crater, Mars. *Paper presented at the 45th Lunar and Planetary Science Conference, The Woodlands, TX*.

Eigenbrode, J. L., Summons, R. E., Steele, A., Freissinet, C., Millan, M., Navarro-González, R., et al. (2018). Organic matter preserved in 3-billion-year-old mudstones at Gale crater, Mars. *Science*, *360*(6393), 1096–1101. https://doi.org/10.1126/science.aas9185

Fox, A. C., Eigenbrode, J. L., & Freeman, K. H. (2019). Radiolysis of macromolecular organic material in Mars-relevant mineral matrices. *Journal of Geophysical Research-Planets*, *124*. https://doi.org/10.1029/2019je006072

Fox, V. K., Bennett, K. A., Bryk, A., Arvidson, R. E., Bristow, T., Dehouck, E., et al. (2020). One year in Glen Torridon: Key results from the Mars Science Laboratory curiosity rover exploration of clay-bearing units. *Paper presented at the 51st Lunar and Planetary Science Conference, The Woodlands, TX*.

Fraeman, A. A., Arvidson, R. E., Catalano, J. G., Grotzinger, J. P., Morris, R. V., Murchie, S. L., et al. (2013). A hematite-bearing layer in Gale Crater, Mars: Mapping and implications for past aqueous conditions. *Geology*, *41*(10), 1103–1106. https://doi.org/10.1130/g34613.1

Fraeman, A. A., Edgar, L. A., Rampe, E. B., Thompson, L. M., Frydenvang, J., Fedo, C. M., et al. (2020). Evidence for a diagenetic origin of Vera Rubin Ridge, Gale Crater, Mars: Summary and synthesis of curiosity's exploration campaign. *Journal of Geophysical Research: Planets*, e2020JE006527. https://doi.org/10.1029/2020JE006527

Fraeman, A. A., Ehlmann, B. L., Arvidson, R. E., Edwards, C. S., Grotzinger, J. P., Milliken, R. E., et al. (2016). The stratigraphy and evolution of lower Mount Sharp from spectral, morphological, and thermophysical orbital data sets. *Journal of Geophysical Research: Planets*, *121*(9), 1713–1736. https://doi.org/10.1002/2016je005095

Franz, H. B., Mahaffy, P. R., Webster, C. R., Flesch, G. J., Raaen, E., Freissinet, C., et al. (2020). Indigenous and exogenous organics and surface-atmosphere cycling inferred from carbon and oxygen isotopes at Gale crater. *Nature Astronomy*. https://doi.org/10.1038/s41550-019-0990-x

Franz, H. B., Trainer, M. G., Wong, M. H., Manning, H. L., Stern, J. C., Mahaffy, P. R., et al. (2014). Analytical techniques for retrieval of atmospheric composition with the quadrupole mass spectrometer of the Sample Analysis at Mars instrument suite on Mars Science Laboratory. *Planetary and Space Science*, *96*, 99–113. https://doi.org/10.1016/j.pss.2014.03.005

Freissinet, C., Glavin, D. P., Mahaffy, P. R., Miller, K. E., Eigenbrode, J. L., Summons, R. E., et al. (2015). Organic molecules in the Sheepbed Mudstone, Gale Crater, Mars. *Journal of Geophysical Research: Planets*, *120*(3), 495–514. https://doi.org/10.1002/2014je004737

Freissinet, C., Knudson, C. A., Graham, H. V., Lewis, J. M. T., Lasue, J., Mcadam, A. C., et al. (2020). Benzoic acid as the preferred precursor for the chlorobenzene detected on Mars: Insights from the unique Cumberland analog investigation. *Planetary Science Journal*, *1*(2), 41. https://doi.org/10.3847/psj/aba690

Fuchs, L. H., Olsen, E., & Jensen, K. J. (1973). *Mineralogy, mineral-chemistry, and composition of the Murchison (C2) meteorite. Smithsonian contributions to the earth sciences*. https://doi.org/10.5479/si.00810274.10.1

Gadalla, A. M. (1984). Kinetics of the decomposition of hydrated oxalates of calcium and magnesium in air. *Thermochimica Acta*, *74*(1–3), 255–272. https://doi.org/10.1016/0040-6031(84)80027-1

Gaillard, F., Michalski, J., Berger, G., McLennan, S. M., & Scaillet, B. (2013). Geochemical reservoirs and timing of sulfur cycling on Mars. *Space Science Reviews*, *174*(1–4), 251–300. https://doi.org/10.1007/s11214-012-9947-4

Galwey, A. K., & Brown, M. E. (1999). *Thermal decomposition of ionic solids: Chemical properties and reactivities of ionic crystalline phases*. Elsevier.

Glavin, D. P., Freissinet, C., Miller, K. E., Eigenbrode, J. L., Brunner, A. E., Buch, A., et al. (2013). Evidence for perchlorates and the origin of chlorinated hydrocarbons detected by SAM at the Rocknest aeolian deposit in Gale Crater. *Journal of Geophysical Research: Planets*, *118*(10), 1955–1973. https://doi.org/10.1002/jgre.20144

Goesmann, F., Brinckerhoff, W. B., Raulin, F., Goetz, W., Danell, R. M., Getty, S. A., et al. (2017). The Mars Organic Molecule Analyzer (MOMA) instrument: Characterization of organic material in martian sediments. *Astrobiology*, *17*(6–7), 655–685. https://doi.org/10.1089/ast.2016.1551

Grotzinger, J. P., Crisp, J., Vasavada, A. R., Anderson, R. C., Baker, C. J., Barry, R., et al. (2012). Mars Science Laboratory mission and science investigation. *Space Science Reviews*, *170*(1–4), 5–56. https://doi.org/10.1007/s11214-012-9892-2

Grotzinger, J. P., Sumner, D. Y., Kah, L. C., Stack, K., Gupta, S., Edgar, L., et al. (2014). A habitable fluvio-lacustrine environment at Yellowknife Bay, Gale Crater, Mars. *Science*, *343*(6169). https://doi.org/10.1126/science.1242777

Hartmann, W. K., Malin, M., McEwen, A., Carr, M., Soderblom, L., Thomas, P., et al. (1999). Evidence for recent volcanism on Mars from crater counts. *Nature*, *397*(6720), 586–589. https://doi.org/10.1038/17545

Hassler, D. M., Zeitlin, C., Wimmer-Schweingruber, R. F., Ehresmann, B., Rafkin, S., Eigenbrode, et al. (2014). Mars' surface radiation environment measured with the Mars Science Laboratory's Curiosity rover. *Science*, *343*(6169), 1244797. https://doi.org/10.1126/science.1244797

Hermankova, P., Hermanek, M., & Zboril, R. (2010). Thermal decomposition of ferric oxalate tetrahydrate in oxidative and inert atmospheres: The role of ferrous oxalate as an intermediate. *European Journal of Inorganic Chemistry*, *2010*(7), 1110–1118. https://doi.org/10.1002/ejic.200900835

Hoffman, J., Chaney, R., & Hammack, H. (2008). Phoenix Mars mission—The thermal evolved gas analyzer. *Journal of the American Society for Mass Spectrometry*, *19*(10), 1377–1383. https://doi.org/10.1016/j.jasms.2008.07.015

Hofmann, B. A., & Bernasconi, S. M. (1998). Review of occurrences and carbon isotope geochemistry of oxalate minerals: Implications for the origin and fate of oxalate in diagenetic and hydrothermal fluids. *Chemical Geology*, *149*(1–2), 127–146. https://doi.org/10.1016/s0009-2541(98)00043-6

Johnston, C. G., & Vestal, J. R. (1993). Biogeochemistry of oxalate in the Antarctic cryptoendolithic lichen-dominated community. *Microbial Ecology*, *25*(3), 305–319. https://doi.org/10.1007/bf00171895

Judd, M. D., Plunkett, B. A., & Pope, M. I. (1974). The thermal decomposition of calcium, sodium, silver and copper(II) acetates. *Journal of Thermal Analysis*, *6*(5), 555–563. https://doi.org/10.1007/bf01911560

Lasne, J., Noblet, A., Szopa, C., Navarro-González, R., Cabane, M., Poch, O., et al. (2016). Oxidants at the surface of Mars: A review in light of recent exploration results. *Astrobiology*, *16*(12), 977–996. https://doi.org/10.1089/ast.2016.1502

Lawson-Wood, K., & Robertson, I. (2016). *Study of the decomposition of calcium oxalate monohydrate using a hyphenated thermogravimetric analyser-FT-IR system (TG-IR)*. PerkinElmer, Inc.

Leshin, L., Mahaffy, P., Webster, C., Cabane, M., Coll, P., Conrad, P., et al. (2013). Volatile, isotope, and organic analysis of martian fines with the Mars Curiosity rover. *Science*, *341*(6153), 1238937. https://doi.org/10.1126/science.1238937

Lewis, J. M. T. (2021). *Data for Lewis et al. pyrolysis of oxalate, acetate, and perchlorate mixtures and the implications for organic salts on Mars*. Harvard Dataverse. https://doi.org/10.7910/DVN/9TULFS

Mahaffy, P. R., Webster, C. R., Cabane, M., Conrad, P. G., Coll, P., Atreya, S. K., et al. (2012). The sample analysis at Mars investigation and instrument suite. *Space Science Reviews*, *170*(1–4), 401–478. https://doi.org/10.1007/s11214-012-9879-z

Marvin, G. G., & Woolaver, L. B. (1945). Thermal decomposition of perchlorates. *Industrial & Engineering Chemistry Analytical Edition*, *17*(8), 474–476. https://doi.org/10.1021/i560144a004

McAdam, A. C., Sutter, B., Archer, P. D., Franz, H. B., Eigenbrode, J. L., & Knudson, C. A. (2020). Constraints on the depositional and diagenetic history of the glen Torridon clay-bearing unit from the Mars science laboratory sample analysis at Mars instrument suite. *Paper presented at the Fall AGU Meeting, San Francisco, CA*.

McAdam, A. C., Sutter, B., Archer, P. D., Franz, H. B., Wong, G. M., Lewis, J. M. T., et al. (2020). Constraints on the mineralogy and geochemistry of the Vera Rubin Ridge, Gale crater, Mars, from Mars Science Laboratory sample analysis at Mars evolved gas analyses. *Journal of Geophysical Research: Planets*, *125*(11), e2019JE006309. https://doi.org/10.1029/2019je006309

McAdie, H. G., & Jervis, J. M. (1970). The pyrolysis of metal acetates. *Thermochimica Acta*, *1*(1), 19–28. https://doi.org/10.1016/0040-6031(70)85025-0

Ming, D. W., Archer, P. D., Glavin, D. P., Eigenbrode, J. L., Franz, H. B., Sutter, B., et al. (2014). Volatile and organic compositions of sedimentary rocks in Yellowknife Bay, Gale Crater, Mars. *Science*, *343*(6169). https://doi.org/10.1126/science.1245267

Minitti, M. E., Kah, L. C., Yingst, R. A., Edgett, K. S., Anderson, R. C., Beegle, L. W., et al. (2013). MAHLI at the Rocknest sand shadow: Science and science-enabling activities. *Journal of Geophysical Research: Planets*, *118*, 2338–2360. https://doi.org/10.1002/2013je004426

Morris, R. V., Vaniman, D. T., Blake, D. F., Gellert, R., Chipera, S. J., Rampe, E. B., et al. (2016). Silicic volcanism on Mars evidenced by tridymite in high-SiO_2 sedimentary rock at Gale crater. *Proceedings of the National Academy of Sciences of the United States of America*, *113*(26), 7071–7076. https://doi.org/10.1073/pnas.1607098113

Nachon, M., Mangold, N., Forni, O., Kah, L. C., Cousin, A., Wiens, R. C., et al. (2017). Chemistry of diagenetic features analyzed by ChemCam at Pahrump Hills, Gale crater, Mars. *Icarus*, *281*, 121–136. https://doi.org/10.1016/j.icarus.2016.08.026

Newsome, D. S. (1980). The water-gas shift reaction. *Catalysis Reviews*, *21*(2), 275–318. https://doi.org/10.1080/03602458008067535

Oró, J., & Holzer, G. (1979). The effects of ultraviolet light on the degradation of organic compounds: A possible explanation for the absence of organic matter on Mars. *Life Sciences and Space Research*, 77–86. https://doi.org/10.1016/b978-0-08-023416-8.50013-1

Pavlov, A. A., Vasilyev, G., Ostryakov, V. M., Pavlov, A. K., & Mahaffy, P. (2012). Degradation of the organic molecules in the shallow subsurface of Mars due to irradiation by cosmic rays. *Geophysical Research Letters*, *39*(13). https://doi.org/10.1029/2012gl052166

Pavlov, A. K., Blinov, A. V., & Konstantinov, A. N. (2002). Sterilization of Martian surface by cosmic radiation. *Planetary and Space Science*, *50*(7–8), 669–673. https://doi.org/10.1016/s0032-0633(01)00113-1

Poch, O., Kaci, S., Stalport, F., Szopa, C., & Coll, P. (2014). Laboratory insights into the chemical and kinetic evolution of several organic molecules under simulated Mars surface UV radiation conditions. *Icarus*, *242*, 50–63. https://doi.org/10.1016/j.icarus.2014.07.014

Rampe, E. B., Blake, D. F., Bristow, T. F., Ming, D. W., Vaniman, D. T., Morris, R. V., et al. (2020). Mineralogy and geochemistry of sedimentary rocks and eolian sediments in Gale crater, Mars: A review after six Earth years of exploration with Curiosity. *Geochemistry*, *80*(2), 125605. https://doi.org/10.1016/j.chemer.2020.125605

Rampe, E. B., Ming, D. W., Blake, D. F., Bristow, T. F., Chipera, S. J., Grotzinger, J. P., et al. (2017). Mineralogy of an ancient lacustrine mudstone succession from the Murray formation, Gale crater, Mars. *Earth and Planetary Science Letters*, *471*, 172–185. https://doi.org/10.1016/j.epsl.2017.04.021

Rull, F., Maurice, S., Hutchinson, I., Moral, A., Perez, C., Diaz, C., et al. (2017). The Raman laser spectrometer for the ExoMars rover mission to Mars. *Astrobiology*, *17*(6–7), 627–654. https://doi.org/10.1089/ast.2016.1567

Saito, N., Sano, H., Tominaga, T., & Ambe, F. (1965). A Mössbauer resonance absorption study of the photolysis and radiolysis of ferric oxalate. *Bulletin of the Chemical Society of Japan*, *38*(4), 681–682. https://doi.org/10.1246/bcsj.38.681

Sasaki, E. (1971). Decomposition of calcium oxalate with sulfuric acid. *The Journal of the Society of Chemical Industry, Japan*, *74*(12), 2426. https://doi.org/10.1246/nikkashi1898.74.12_2426

Steele, A., Benning, L. G., Wirth, R., Siljeström, S., Fries, M. D., Hauri, E., et al. (2018). Organic synthesis on Mars by electrochemical reduction of CO_2. *Science Advances*, *4*(10), eaat5118. https://doi.org/10.1126/sciadv.aat5118

Steele, A., McCubbin, F. M., & Fries, M. D. (2016). The provenance, formation, and implications of reduced carbon phases in Martian meteorites. *Meteoritics & Planetary Sciences*, *51*(11), 2203–2225. https://doi.org/10.1111/maps.12670

Steele, A., McCubbin, F. M., Fries, M., Kater, L., Boctor, N. Z., Fogel, M. L., et al. (2012). A reduced organic carbon component in martian basalts. *Science*, *337*(6091), 212–215. https://doi.org/10.1126/science.1220715

Steininger, H., Goesmann, F., & Goetz, W. (2012). Influence of magnesium perchlorate on the pyrolysis of organic compounds in Mars analogue soils. *Planetary and Space Science*, *71*(1), 9–17. https://doi.org/10.1016/j.pss.2012.06.015

Stern, J. C., Sutter, B., Archer, P. D., Eigenbrode, J. L., McAdam, A. C., Franz, H. B., et al. (2018). Major volatiles evolved from eolian materials in Gale crater. *Geophysical Research Letters*, *45*(19), 10–240. https://doi.org/10.1029/2018gl079059

Sutter, B., Boynton, W. V., Ming, D. W., Niles, P. B., Morris, R. V., Golden, D. C., et al. (2012). The detection of carbonate in the martian soil at the Phoenix Landing site: A laboratory investigation and comparison with the Thermal and Evolved Gas Analyzer (TEGA) data. *Icarus*, *218*(1), 290–296. https://doi.org/10.1016/j.icarus.2011.12.002

Sutter, B., McAdam, A. C., Achilles, C. N., Rampe, E. B., Archer, P. D., Thompson, L. M., et al. (2020). Aqueous processes and microbial habitability of Gale crater sediments from the blunts point to the Glenn Torridon clay unit. *Paper presented at the 51st Lunar and Planetary Science Conference, The Woodlands, TX*.

Sutter, B., McAdam, A. C., Archer, P. D., Ming, D. W., Eigenbrode, J. L., & Rampe, E. B. (2020). Geochemical processes along and above the Glen Torridon/Greenheugh pediment, unconformity, Gale crater, Mars: Results from the sample analysis at Mars instrument. *Paper presented at the Fall AGU Meeting, San Francisco, CA*.

Sutter, B., McAdam, A. C., Mahaffy, P. R., Ming, D. W., Edgett, K. S., Rampe, E. B., et al. (2017). Evolved gas analyses of sedimentary rocks and eolian sediment in Gale Crater, Mars: Results of the Curiosity rover's sample analysis at Mars instrument from Yellowknife Bay to the Namib Dune. *Journal of Geophysical Research: Planets*, *122*(12), 2574–2609. https://doi.org/10.1002/2016je005225

Szopa, C., Freissinet, C., Glavin, D. P., Millan, M., Buch, A., Franz, H. B., et al. (2020). First detections of dichlorobenzene isomers and trichloromethylpropane from organic matter indigenous to Mars mudstone in Gale Crater, Mars: Results from the sample analysis at Mars instrument onboard the curiosity rover. *Astrobiology*, *20*(2), 292–306. https://doi.org/10.1089/ast.2018.1908

Thorpe, M. T., Bristow, T. F., Rampe, E. B., Grotzinger, J. P., Fox, V. K., Bennett, K. A., et al. (2020). Glen Torridon mineralogy and the sedimentary history of the clay mineral bearing unit. *Paper presented at the 51st Lunar and Planetary Science Conference, The Woodlands, TX*.

Treiman, A. H., Bish, D. L., Vaniman, D. T., Chipera, S. J., Blake, D. F., Ming, D. W., et al. (2016). Mineralogy, provenance, and diagenesis of a potassic basaltic sandstone on Mars: CheMin X-ray diffraction of the Windjana sample (Kimberley area, Gale Crater). *Journal of Geophysical Research: Planets*, *121*, 75–106. https://doi.org/10.1002/2015je004932

Vaniman, D. T., Bish, D. L., Ming, D. W., Bristow, T. F., Morris, R. V., Blake, D. F., et al. (2014). Mineralogy of a mudstone at Yellowknife Bay, Gale crater, Mars. *Science*, *343*(6169). https://doi.org/10.1126/science.1243480

Vedyagin, A. A., Mishakov, I. V., & Tsyrulnikov, P. G. (2016). The features of the CO disproportionation reaction over iron-containing catalysts prepared by different methods. *Reaction Kinetics, Mechanisms and Catalysis*, *117*(1), 35–46. https://doi.org/10.1007/s11144-015-0936-y

Wanjun, T., & Donghua, C. (2007). Mechanism of thermal decomposition of cobalt acetate tetrahydrate. *Chemical Papers*, *61*(4), 329–332. https://doi.org/10.2478/s11696-007-0042-3

Wiens, R. C., Maurice, S., Robinson, S. H., Nelson, A. E., Cais, P., Bernardi, P., et al. (2021). The SuperCam instrument suite on the NASA Mars 2020 rover: Body unit and combined system tests. *Space Science Reviews*, *217*(1), 1–87. https://doi.org/10.1007/s11214-020-00777-5

Williford, K. H., Farley, K. A., Stack, K. M., Allwood, A. C., Beaty, D., Beegle, L. W., et al. (2018). The NASA Mars 2020 rover mission and the search for extraterrestrial life. In *Habitability to life on Mars* (pp. 275–308). https://doi.org/10.1016/B978-0-12-809935-3.00010-4

Yen, A. S., Ming, D. W., Vaniman, D. T., Gellert, R., Blake, D. F., Morris, R. V., et al. (2017). Multiple stages of aqueous alteration along fractures in mudstone and sandstone strata in Gale Crater, Mars. *Earth and Planetary Science Letters*, *471*, 186–198. https://doi.org/10.1016/j.epsl.2017.04.033